



HAL
open science

Distribution of transparent exopolymer particles (TEP) in distinct regions of the Southern Ocean

Eva Ortega-Retuerta, Marina Zamanillo, Eva Ortega-Retuerta, Sdena Nunes,
Marta Estrada, María Montserrat Sala, Sarah-Jeanne Royer, Daffne C
López-Sandoval, Mikhail Emelianov, Dolors Vaqué, et al.

► **To cite this version:**

Eva Ortega-Retuerta, Marina Zamanillo, Eva Ortega-Retuerta, Sdena Nunes, Marta Estrada, et al..
Distribution of transparent exopolymer particles (TEP) in distinct regions of the Southern Ocean.
Science of the Total Environment, 2019, 10.1016/j.scitotenv.2019.06.524 . hal-04003689

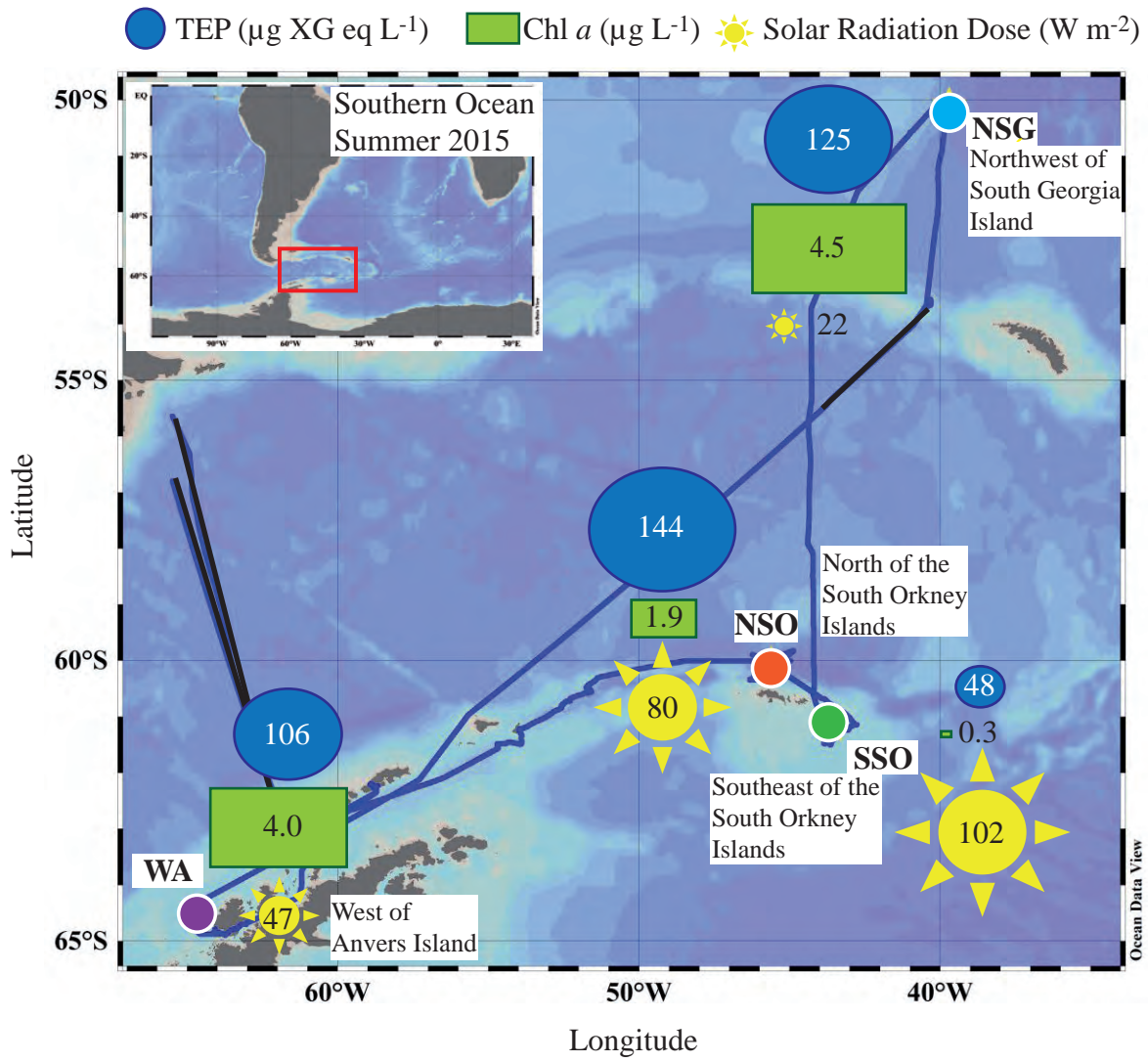
HAL Id: hal-04003689

<https://hal.science/hal-04003689>

Submitted on 29 May 2024

HAL is a multi-disciplinary open access archive for the deposit and dissemination of scientific research documents, whether they are published or not. The documents may come from teaching and research institutions in France or abroad, or from public or private research centers.

L'archive ouverte pluridisciplinaire **HAL**, est destinée au dépôt et à la diffusion de documents scientifiques de niveau recherche, publiés ou non, émanant des établissements d'enseignement et de recherche français ou étrangers, des laboratoires publics ou privés.



25 **Abstract**

26 Transparent exopolymer particles (TEP) are an abundant class of suspended organic
27 particles, mainly formed by polysaccharides, which play important roles in
28 biogeochemical and ecological processes in the ocean. In this study we investigated
29 horizontal and vertical TEP distributions (within the euphotic layer, including the upper
30 surface) and their short-term variability along with a suite of environmental and
31 biological variables in four distinct regions of the Southern Ocean. TEP concentrations
32 in the surface (4 m) averaged $102.3 \pm 40.4 \mu\text{g XG eq L}^{-1}$ and typically decreased with
33 depth. Chlorophyll *a* (Chl *a*) concentration was a better predictor of TEP variability
34 across the horizontal ($R^2 = 0.66$, $p < 0.001$) and vertical ($R^2 = 0.74$, $p < 0.001$) scales than
35 prokaryotic heterotrophic abundance and production. Incubation experiments further
36 confirmed the main role of phytoplankton as TEP producers. The highest surface TEP
37 concentrations were found north of the South Orkney Islands ($144.4 \pm 21.7 \mu\text{g XG eq L}^{-1}$),
38 where the phytoplankton was dominated by cryptophytes and haptophytes; however,
39 the highest TEP:Chl *a* ratios were found south of these islands ($153.4 \pm 29.8 \mu\text{g XG eq}$
40 $(\mu\text{g Chl } a)^{-1}$), compared to a mean of $79.3 \pm 54.9 \mu\text{g XG eq } (\mu\text{g Chl } a)^{-1}$ in the whole
41 cruise, in association with haptophyte dominance, proximity of sea ice and high
42 exposure to solar radiation. TEP were generally enriched in the upper surface (10 cm)
43 respect to 4 m, despite a lack of biomass enrichment, suggesting either upward transport
44 by positive buoyancy or bubble scavenging, or higher production at the upper surface
45 by light stress or aggregation. TEP concentrations did not present any significant cyclic
46 diel pattern. Altogether, our results suggest that photobiological stress, sea ice melt and
47 turbulence add to phytoplankton productivity in driving TEP distribution across the
48 Antarctic Peninsula area and Atlantic sector of the Southern Ocean.

49 **Keywords:** Transparent exopolymer particles, phytoplankton, prokaryotes, solar
50 radiation dose, Southern Ocean

51

52 **1 Introduction**

53 Transparent exopolymer particles (TEP) are gel-like organic particles stainable with
54 Alcian Blue, a specific dye for acidic polysaccharides (Alldredge et al., 1993), that have
55 deserved attention due to their influence in biogeochemical and ecological processes
56 (Passow, 2002b). TEP are partly formed by the abiotic self-assembly from dissolved
57 precursors (Chin et al., 1998; Orellana and Verdugo, 2003), thus connecting the
58 dissolved to particulate organic matter continuum (Engel et al., 2004). In addition, TEP
59 affect the biological carbon pump, not only because TEP by themselves may comprise a
60 mean of 5-10 % of primary production synthates (Mari et al., 2017) that can sink into
61 the deep ocean, but also because they promote particle aggregation (Engel et al., 2004),
62 thus favouring the sinking of marine snow to the deep ocean (Burd and Jackson, 2009).
63 TEP also influence air-sea gas exchanges like that of carbon dioxide (CO₂) (Wurl et al.,
64 2016; Jenkinson et al., 2018), since they tend to accumulate at the surface microlayer
65 (SML, the uppermost water layer, Cunliffe et al. (2013)), either after ascending through
66 the water column (Azetsu-Scott and Passow, 2004) or upon direct production in this
67 layer (Wurl et al., 2011b).

68 Phytoplankton are believed to be the main source of TEP and their precursors
69 (Alldredge et al., 1993; Passow, 2002b; Van Oostende et al., 2012; Engel et al., 2015),
70 being diatoms (Passow et al., 1994; Mari and Burd, 1998; Passow et al., 2001; Passow,
71 2002a) and haptophytes, like *Phaeocystis* (Hong et al., 1997), the groups that seem to
72 release larger amounts. Prokaryotic heterotrophs (Stoderegger and Herndl, 1999;

73 Ortega-Retuerta et al., 2010) and other organisms, such as suspension feeders
74 (Heinonen et al., 2007), zooplankton (Prieto et al., 2001) and seagrass (Iuculano et al.,
75 2017a), can also produce TEP.

76 Sinks of TEP comprise photolysis by UV radiation (Ortega-Retuerta et al., 2009a),
77 sinking to the deep ocean, entrance to the atmosphere (Kuznetsova et al., 2005), and
78 degradation and consumption by microorganisms (Ling and Alldredge, 2003). Many
79 variables influence either sources, sinks or both, hindering the prediction of TEP
80 distribution in the ocean. For example, high solar radiation has a dual effect; it
81 stimulates TEP release by microbes (Iuculano et al., 2017b) but also causes TEP
82 photolysis (Ortega-Retuerta et al., 2009a) or affect positively (Shammi et al., 2017) or
83 negatively (Orellana and Verdugo, 2003) the abiotic self-assembly of dissolved
84 exopolymers into TEP. Other variables such as temperature (Nicolaus et al., 1999;
85 Claquin et al., 2008), CO₂ concentration (Engel, 2002), nutrient availability (Mari et al.,
86 2005) and viral infections (Nissimov et al., 2018) can also influence TEP cycling.
87 Moreover, the TEP production per phytoplankton biomass increases along the bloom
88 stages (Pedrotti et al., 2010), thus adding complexity to the TEP dynamics.

89 The Southern Ocean (SO) is characterized by the presence of the Antarctic Circumpolar
90 Current, which connects the waters of the Pacific, Indian and Atlantic Oceans, and by
91 having strong upwellings that enrich surface waters with macronutrients (Sarmiento et
92 al., 2004). Productivity is generally limited by the lack of iron in combination with deep
93 surface mixing and low light and temperature (Moore et al., 2013; Hoppe et al., 2017),
94 although some regions are locally supplied with iron, particularly in the vicinity of
95 islands (Morris and Sanders, 2011).

96 The study of TEP distributions in the SO is of particular importance in light of these
97 ocean's peculiarities. The SO is considered the largest region for anthropogenic CO₂
98 sequestration in the world (Frölicher et al., 2015), especially around the island systems
99 (Pollard 2009), through higher CO₂ solubility in cold waters and a relatively high
100 particulate organic carbon (POC) surface export flux in comparison to lower latitudes
101 (Boyd and Trull, 2007; Marinov et al., 2008). Indeed, C export fluxes have been
102 reported to attain 30-50 % of net primary production (Buesseler, 2001). Since TEP may
103 account for an important fraction of POC mass (Engel, 2004; Zamanillo et al., 2019)
104 and export flux (Passow, 2002b; Wurl et al., 2011a), their study in the SO is important
105 to better predict the magnitude of the biological carbon pump and the future dynamics
106 of atmospheric CO₂.

107 In this study we describe the horizontal and vertical (within the euphotic layer)
108 distributions, and short-term (diel) variability of TEP, along with relevant physical,
109 chemical and biological variables, in four distinct regions of the SO. The four regions
110 were characterized by distinct phytoplankton communities, bloom stages and
111 environmental and ecological properties. Our objectives were: (a) to identify the main
112 drivers of TEP distribution across contrasting environmental conditions, both
113 horizontally and vertically, and (b) to examine the short-term temporal variability of
114 TEP and biological variables, over diel cycles. Data co-variation analyses and
115 experimental incubations were conducted to ascertain the role of microorganisms
116 (phytoplankton vs. heterotrophic prokaryotes) in TEP production.

117

118 **2. Material and methods**

119 **2.1 Study site and sampling**

120 Sampling was performed during the PEGASO cruise, on board the Spanish R/V
121 *Hespérides*, conducted from 7th January to 3rd February, in the austral summer of 2015.
122 A total of 70 stations were sampled within the Southern Ocean (Fig. S1). Four regions
123 were occupied for several days, following a Lagrangian approach; the north of the South
124 Orkney Islands (NSO), the southeast of the South Orkney Islands (SSO), the northwest
125 of South Georgia (NSG) and the west of Anvers Island (WA). NSO, NSG and WA were
126 selected due to their relatively high chlorophyll *a* (Chl *a*) concentrations, different
127 nutrient conditions and relatively slow currents with the absence of stable direction
128 (Nunes et al., 2019). SSO was selected for its vicinity to the sea ice edge. In order to
129 track the studied water bodies, WOCE (World Ocean Circulation Experiment) standard
130 drifters provided with Iridium communication system were used in the NSO, NSG and
131 WA regions; in SSO, two icebergs were used as natural Lagrangian drifters.

132 During the transit between the regions, seawater was collected from 4 m depth using the
133 ship's underway pump (BKMKC-10.11. Tecnum, Manresa, Spain), approximately at
134 9:00 and 15:00 local time (UTC-3). During the Lagrangian occupation of the main
135 stations, CTD casts were carried out using a SBE 911 Plus probe attached to a rosette of
136 24 12-L PVC Niskin bottles, at least once a day, generally at 9:00 and 15:00 local time
137 (UTC-3). The underway sampling was used when conditions were too rough for CTD
138 launch (a total of 3 times). A 36-h cycle was also sampled in each region, with CTD
139 casts every 4 h, generally from 9:30 to 17:00 (solar times) the day after. NASA Solar
140 Calculator (<https://www.esrl.noaa.gov/gmd/grad/solcalc/>, accessed on 15 December
141 2017) was used to perform solar time calculations (Nunes et al., 2019). The position of
142 the main hydrographic fronts was determined as described in Nunes et al. (2019).

143 TEP, major nutrients, POC, prokaryotic heterotrophic abundance (PHA) and production
144 (PHP), primary production (PP), phytoplankton recount and identification by

145 microscopy and flow cytometry, extracellular enzyme activities and virus concentrations
146 were analyzed in surface samples. At 7 stations (three in NSO, two in SSO, one in NSG
147 and one in WA), Chl *a*, phytoplankton pigment analyses and PHA were carried out for 6
148 different depths, generally from 4 to 120-150 m, while TEP were analysed for 4 depths,
149 from 4 m to the second deepest depth. In some of these stations, phytoplankton
150 identification and recount by microscopy and flow cytometry were done from 2 to 4
151 depths, including the depth of maximum fluorescence. Mixed layer depth (MLD)
152 estimation was done from CTD profiles following Monterey and Levitus (1997).

153 A total of 14 samples (one in the transit between regions, seven in NSO, four in SSO,
154 one in NSG and one in WA) were collected from the upper surface (10 cm) using a
155 zodiac boat, away and upstream from the ship to avoid contamination. Sampling was
156 carried out with a device of our own design, consisting of a 50 mL glass syringe
157 connected to a PTFE tube 1.5 m long, whose other end was fixed onto a floating item so
158 that the inlet of the tube remained at a depth of 10 cm regardless of the motion of the
159 sea surface. All material was prewashed with HCl (10 %) and Milli-Q water. Typical
160 collected volume was 400 mL; usually, sampling took place around 10:00 local time
161 (UTC-3) during standard stations and at 11:00 and 17:00 local time during intensive
162 day-night cycles. TEP, Chl *a*, PHA, PHP and extracellular enzyme activities were
163 analysed at the upper surface. In order to compare these measurements with those at the
164 nominal surface (4 m depth of the nearest CTD casts), we calculated an enrichment
165 factor (EF_{us}), defined as:

$$EF_{us} = \frac{[X]_{\text{upper surface}}}{[X]_{\text{surface}}}$$

166 where $[X]$ is the concentration of a given variable, in the upper surface and surface
167 respectively. $EF_{us} > 1$ indicates enrichment of a component in the upper surface and

168 $EF_{us} < 1$ indicates depletion. It is worth mentioning that the time difference between the
169 upper surface sampling and the nearest surface sampling was 1-3 h. When the upper
170 surface sampling occurred exactly between two CTD casts, the average of the two was
171 used.

172 **2.2 Physical measurements**

173 Surface temperature and salinity were obtained continuously with the SBE21 Sea Cat
174 Thermosalinograph, while vertical profiles were recorded down to 400 m with a CTD
175 SBE911 plus. Average diffuse attenuation coefficient in the euphotic zone for PAR
176 broadband (400-700 nm; K_d (PAR)), from both CTD and PRR-800 vertical profiles of
177 downwelling spectral irradiance (E_d), were determined as the slope of the linear
178 regression between logarithmic irradiances and depth. Prior to analysis, the data were
179 carefully examined for irregularities (Mueller et al., 2003). Near-surface noise caused
180 by smooth waves and ripples was eliminated from E_d (PAR) profiles. The obtained R^2
181 of regression analyses were always above 0.98 at all evaluated casts. The depth of the
182 euphotic layer was then calculated as $4.605/K_d$ (PAR), being the depth at which K_d
183 (PAR) is reduced to 1 % of its value just below the surface. Solar radiation dose was
184 calculated in every station using the following formula:

$$185 \text{ Solar radiation dose} = \frac{I}{K_d(\text{PAR}) \times \text{MLD}} \times (1 - e^{(-K_d(\text{PAR}) \times \text{MLD})})$$

186 where, I is the average surface intensity radiation ($W\ m^{-2}$) in the 24 h previous to
187 sampling, K_d (PAR) is the average diffuse attenuation coefficient in the euphotic zone
188 for PAR broadband (m^{-1}), and MLD is the mixed layer depth (m).

189 **2.3 Chemical and biological analyses**

190 **2.3.1 Particulate organic matter (TEP and POC)**

191 TEP were analysed by spectrophotometry following the method proposed by Passow
192 and Alldredge (1995). Samples were filtered under low constant filtration pressure
193 (~150 mm Hg) in duplicate (200-550 mL) using 25 mm diameter polycarbonate filters
194 (DHI) with a pore size of 0.4 μm . All sampling material was pre-washed with HCl (10
195 %) and Milli-Q water. Filters were immediately stained with 500 μL of Alcian Blue
196 solution (0.02 %, pH 2.5) for 5 s, and then rinsed with Milli-Q water. Two empty filters
197 (blanks) were taken at every station and stained in the same way. All filters remained
198 frozen until further processing some months later at the home laboratory. There, filters
199 were soaked in 80 % sulfuric acid (5 mL) for 3 h and shaken intermittently. Absorbance
200 of the acid solutions was then measured at 787 nm with a Varian Cary 100 Bio
201 spectrophotometer. The absorbance of filter blanks, taken in duplicate for every batch of
202 samples, was subtracted from the absorbance of samples. Calibration of the Alcian Blue
203 solution was conducted immediately after the cruise using xanthan gum (XG) solution
204 as a standard. The detection limit was set to 0.045 absorbance units, and the mean range
205 between duplicates was 25.5 %. TEP carbon content (TEP-C) was estimated using the
206 conversion factor of 0.51 μg TEP-C per μg XG eq (Engel and Passow, 2001).

207 For POC analysis, we filtered water samples (1000 mL) through pre-combusted (4 h,
208 450 $^{\circ}\text{C}$) GF/F glass fiber filters (Whatman) that remained frozen (-20 $^{\circ}\text{C}$) until further
209 processing. Filters were dried, acidified to remove carbonates and analyzed with an
210 elemental analyser (Perkin-Elmer 2400 CHN).

211 **2.3.2 Chl *a***

212 For Chl *a* analyses, 250 mL of sea water were filtered through 25 mm diameter glass
213 filters (Whatman GF/F). Filters were stored frozen (-20 $^{\circ}\text{C}$) until further processing in
214 the home laboratory. Ninety % acetone was used to extract pigments at 4 $^{\circ}\text{C}$ in the dark

215 for 24 h. The procedure of Yentsch and Menzel (1963) was followed to measure
216 fluorescence of extracts, with a calibrated Turner Designs fluorometer.

217 **2.3.3 Inorganic nutrients**

218 To analyse dissolved inorganic nutrients (nitrate, phosphate and silicate), unfiltered
219 water samples were stored frozen (-20 °C) in 10 mL sterile polypropylene bottles and
220 further processed in the home laboratory using a Skalar Autoanalyser and the standard
221 segmented flow analyses with colorimetric detection elemental analyser (Hansen and
222 Grasshoff, 1983).

223 **2.3.4 HPLC pigment analysis and CHEMTAX**

224 As described in Nunes et al. (2019), HPLC was used to determine pigment composition,
225 following Latasa (2014). Thirty-two pigments were identified at 474 and 664 nm.
226 Version 1.95 of the CHEMTAX chemical taxonomy software was used to derive the
227 contribution of microalgal groups to the total Chl *a* biomass (ng Chl *a* L⁻¹), from
228 pigment data (Mackey et al., 1996). Seven pigmentary classes were quantified:
229 chlorophytes, cryptophytes, diatoms, dinoflagellates, haptophytes, prasinophytes and
230 pelagophytes. Pigments were also used as indicators of phytoplankton
231 photoacclimation. Diadinoxanthin (Ddx) is the main light-protecting pigment in
232 diatoms, dinoflagellates, haptophytes and pelagophytes. The Ddx:LHC ratio, between
233 Ddx and the sum of the main light-harvesting carotenoids (LHC: fucoxanthin, 19'-
234 butanoyloxyfucoxanthin, 19'-hexanoyloxyfucoxanthin and peridinin) was measured,
235 since it varies with the exposure of phytoplankton to underwater solar radiation
236 (Higgins et al., 2011; Nunes et al., 2019).

237 **2.3.5 Picophytoplankton abundance and biomass**

238 Abundance of picoplankton was determined by flow cytometry in a FACS Calibur
239 instrument (Becton and Dickinson), as described in Zamanillo et al. (2019).
240 *Prochlorococcus* and *Synechococcus* were undetectable in all samples. Biomass of
241 picoeukaryotic algae was measured using the average C:cell conversion factor from
242 Simó et al. (2009): $1319 \pm 813 \text{ fg C cell}^{-1}$.

243 **2.3.6 Microphytoplankton identification and biomass**

244 We identified and quantified phytoplankton groups by microscopy, using the inverted
245 microscope method (Utermöhl, 1958) as described in Nunes et al. (2019). We measured
246 the biomass of phytoplankton groups using conversion equations of Menden-Deuer and
247 Lessard (2000), as explained in Zamanillo et al. (2019). The total biomass of
248 phytoplankton (Phyto B) was obtained as the sum of all the phytoplankton groups.

249 **2.3.7 Primary production (PP)**

250 Phytoplankton primary production rates at four depths within the water column were
251 determined by using $20 \mu\text{Ci}$ of $\text{NaH}^{14}\text{CO}_3$ (Steeman-Nielsen, 1952) in a series of 2-3
252 hours-long, on-deck incubations in flowing surface seawater and under simulated in situ
253 light levels. During the 36-h cycles, water was collected directly from the Niskin bottles
254 in 72 mL acid-washed polystyrene bottles at different sampling times (8:30, 16:30, 4:00
255 and 12:00 local time (UTC-3)). PP rates were estimated from radioisotope incorporation
256 into particles retained on a $0.2 \mu\text{m}$ PC filter, after acid removal of inorganic ^{14}C and
257 subtraction of the incorporation in dark controls. Daily rates were estimated by taking
258 into account the daylight period.

259 **2.3.8 Prokaryotic heterotrophic abundance (PHA) and production (PHP)**

260 Prokaryotic heterotrophic abundance (PHA) was determined by flow cytometry
261 following standard methods, after fixation with 1 % paraformaldehyde plus 0.05 %
262 glutaraldehyde (Gasol and del Giorgio, 2000). PHP was estimated following the
263 Kirchman et al. (1985) method after the centrifugation method described in Smith and
264 Azam (1992). Final leucine concentration was 40 nM. The incubations were carried out
265 in the dark at in situ temperature in a water bath during 3-4 h.

266 **2.3.9 Viral abundance (VA)**

267 Viral abundance was quantified using flow cytometry (Brussaard, 2004). We
268 discriminated three viral subpopulations with different green fluorescence properties
269 (Brussaard et al., 2010) and classified them as “phage viruses” (PV), “large viruses”
270 (LV) and “total viruses” (TV).

271 **2.3.10 Extracellular enzyme activities**

272 We determined the activity of the extracellular enzymes β -glucosidase, esterase and
273 fucosidase following the method detailed in Sala et al. (2016).

274 **2.3.11 Maximum quantum efficiency of photosystem II photochemistry ($F_v:F_m$)**

275 Maximum quantum efficiency of photosystem II photochemistry ($F_v:F_m$) was measured
276 using a Fast Repetition Rate fluorometer (FRRf; FASTracka, Chelsea Technologies,
277 Surrey, UK) on continuous seawater pumped from ca. 4 m deep, as described in Royer
278 et al. (2015).

279 **2.4 TEP production by microbes during experimental incubations**

280 To examine TEP production by microbes (phytoplankton and heterotrophic
281 prokaryotes), we conducted two incubation experiments using surface water (4 m) from

282 the NSO (Experiment NSO) and the NSG (Experiment NSG). Seawater was prefiltered
283 through 200 μm to exclude the presence of mesozooplankton. Each experiment consisted
284 of two treatments: 1) unfiltered seawater (total (T) treatment), 2) seawater filtered
285 through 0.8 μm pore-size Nucleopore filters to exclude most phytoplankton and
286 heterotrophic flagellates, leaving mainly prokaryotes (prokaryotic (P) treatment). Both
287 treatments were set up in triplicates in 25 L teflonated containers under in situ irradiance
288 and temperature conditions. Treatments were incubated for 8 and 13 days for the
289 experiments NSO and NSG, respectively. Experiment NSO was sampled at initial time
290 (t_0) and after 3 (t_1) and 8 (t_2) days, and the experiment NSG was sampled at initial time
291 (t_0) and after 2 (t_1) and 13 (t_2) days. The variables analysed were TEP, PHP and Chl *a*,
292 and we calculated TEP production rate per growth rate (ΔTEP : $\Delta\text{Chl } a$).

293 **2.5 Statistical analyses**

294 The packages *lmodel2* and *ggplot2* of R software were used to test for covariations and
295 to study the potential control of variables on TEP distribution in this study. Bivariate
296 analyses (ordinary least squares, OLS) between TEP concentrations and different
297 chemical, physical and biological variables were used to determine their main
298 predictors. Although ranged major axis (RMA) regression would have been more
299 suitable, due to the presence of errors in our dependent and independent variables, we
300 performed OLS regressions to better compare the slopes between our study and others
301 present in the literature. We used pairwise Spearman correlation analyses to compare
302 different variables in the upper surface (10 cm) and in the surface (4 m). The data were
303 log-transformed to fulfil the requirements of parametric tests. Non-parametric ANOVA
304 followed by post-hoc tests (Tukey) were carried out to compare variables among the
305 four regions. Principal component analysis (PCA) (*devtools* and *ggbiplot* packages in R)
306 was applied to all samples after centering and scaling variables. One PCA was done

307 with a total number of 21 physical, chemical and biological variables, TEP included,
308 while the other one was done replacing TEP and Chl *a* by the TEP:Chl *a* ratio, which is
309 indicative of how prone the plankton community was to net TEP production. The map
310 in Fig. S1 was produced using the Ocean Data View software (version 4) (Schlitzer,
311 2017). The rest of plots were drawn using R programming software (version 3.5.1).

312

313 **3 Results**

314 **3.1 General characterization of sea surface waters**

315 The four study regions (NSO, SSO, NSG and WA, Fig. S1) presented distinct physical,
316 chemical and biological properties, summarized in Table 1. Surface temperatures in the
317 whole transect ranged from -0.9 to 5.1 °C and salinity varied over a narrow range (33.1-
318 34.2). Surface nitrate concentrations ranged from 14.6 to 32.5 $\mu\text{mol L}^{-1}$ and covaried
319 with those of phosphate (1.0-2.5 $\mu\text{mol L}^{-1}$). Silicate concentrations were significantly
320 lower in the NSG region ($2.0 \pm 0.4 \mu\text{mol L}^{-1}$) than in the other three regions (48.1 ± 4.2
321 $\mu\text{mol L}^{-1}$). Within the whole transect, surface Chl *a* concentrations ranged between 0.28
322 and 8.95 $\mu\text{g L}^{-1}$ and averaged $2.36 \pm 1.92 \mu\text{g L}^{-1}$, with a coefficient of variation of 81 %.
323 PHA ranged from 1.60 to $8.44 \times 10^5 \text{ cells mL}^{-1}$, while PHP ranged between 0.09 and
324 2.65 $\text{mg C m}^{-3} \text{ d}^{-1}$. POC ranged from 3.85 to 25.63 $\mu\text{mol L}^{-1}$ and was higher in NSG and
325 WA (11.37-25.63 $\mu\text{mol L}^{-1}$). Primary production was highest in the NSG, averaging
326 $111.6 \pm 85.4 \text{ mg C m}^{-3} \text{ d}^{-1}$, while in the other three regions it averaged $16.2 \pm 15.8 \text{ mg C}$
327 $\text{m}^{-3} \text{ d}^{-1}$, being lower in the SSO ($3.7 \pm 0.8 \text{ mg C m}^{-3} \text{ d}^{-1}$). Solar radiation dose and
328 Ddx:LHC ratio were higher in the NSO and SSO regions, whereas $F_v:F_m$ was lower in
329 these regions.

330 The NSO was located within a meander of the Southern Boundary of the Antarctic
331 Circumpolar Current (Fig. S1) and two months before sampling, this region was
332 covered by > 25 % of sea ice (<https://seaice.uni-bremen.de/start/>). The average values of
333 the surface temperature were 0.59 ± 0.15 °C (Fig. S2). The Chl *a* concentration
334 averaged 1.87 ± 0.23 $\mu\text{g L}^{-1}$ (Fig. 1), and phytoplankton was dominated by
335 cryptophytes, haptophytes and diatoms (Fig. S2). The main planktonic cells identified
336 by microscopy at the surface of this region included the diatoms *Corethron pennatum*,
337 *Fragilariopsis* spp. and *Thalassiosira* spp., unidentified autotrophic cryptophytes and
338 nanoflagellates, and heterotrophic (like *Gyrodinium* spp.) and autotrophic
339 dinoflagellates (Nunes et al., 2019).

340 The SSO was placed north of the Weddell Front (Fig. S1). During the sampling month,
341 the ice cover was > 25 % in the region (<https://seaice.uni-bremen.de/start/>) (Nunes et al.,
342 2019). The month before, the ice cover was > 50 %; therefore, we sampled waters of the
343 receding ice edge. The surface temperature was the lowest among the four regions (-
344 0.75 ± 0.11 °C). Surface Chl *a* averaged 0.32 ± 0.06 $\mu\text{g L}^{-1}$, i.e., significantly ($p < 0.05$)
345 lower than in the other regions (Fig. 1). Phytoplankton was dominated by haptophytes,
346 followed by cryptophytes, chlorophytes and diatoms (Fig. S2). The main planktonic
347 cells identified by microscopy were the same as in the NSO but with a higher proportion
348 of *Fragilariopsis* spp., a characteristic diatom marker of sea ice influence. The SSO
349 presented the highest Ddx:LHC ratio (0.58 ± 0.09 ; Fig. 1) and the lowest $F_v:F_m$ ratio
350 (0.16 ± 0.05), consistently indicating exposure to higher solar radiation intensities in a
351 shallower mixed layer (Table 1).

352 The NSG was located right south of the Polar Front, north of the subAntarctic South
353 Georgia Islands (Fig. S1). Sea surface temperature was the highest among regions (4.77
354 ± 0.45 °C), and the MLD was deepest. The relatively low silicate concentrations found

355 in this region coincided with the dominance of well-silicified diatoms in the
356 phytoplankton community (like *Eucampia Antarctica*, *Thalassiosira* and *Porosira* spp.
357 and *Odontella weissflogii*; Fig. S2) and a smaller proportion of haptophytes and
358 pelagophytes. Surface Chl *a* concentration averaged $4.59 \pm 1.97 \mu\text{g L}^{-1}$ (Fig. 1). The
359 phytoplankton community was complemented by haptophytes and pelagophytes. Total
360 viral abundances (TVA), PHP, PHA and $F_v:F_m$ were significantly higher ($p < 0.05$) in
361 this region than in the others, whereas the solar radiation dose and Ddx:LHC were the
362 lowest.

363 The WA region was placed at the southernmost limit of the Antarctic Circumpolar
364 Current (Southern Boundary) (Fig. S1). The average surface temperature was $1.46 \pm$
365 $0.09 \text{ }^\circ\text{C}$. Chl *a* concentration was slightly lower than in the NSG, with an average of
366 $4.05 \pm 0.48 \mu\text{g L}^{-1}$ (Fig. 1). The phytoplankton community was dominated by
367 cryptophytes, haptophytes and diatoms (Fig. S2).

368 **3.2 TEP concentrations, TEP:Chl *a*, TEP:Phyto B and TEP:PP ratios and** 369 **contribution of TEP to POC in the sea surface of the study regions**

370 Surface TEP concentrations in the entire study regions and transects ranged from 39.2
371 to $177.6 \mu\text{g XG eq L}^{-1}$ and averaged $102.3 \pm 40.4 \mu\text{g XG eq L}^{-1}$, with a coefficient of
372 variation of 39 %. Mean TEP concentrations were significantly different among regions
373 ($p < 0.05$; Table 1). NSO presented the maximum TEP concentrations ($144.4 \pm 21.7 \mu\text{g}$
374 XG eq L^{-1}) and SSO presented the lowest ones ($48.1 \pm 6.5 \mu\text{g XG eq L}^{-1}$), while NSG
375 and WA presented similar TEP concentrations (125.5 ± 21.1 and $111.6 \pm 13.0 \mu\text{g XG eq}$
376 L^{-1} , respectively; Fig. 1).

377 The TEP:Chl *a* ratios were also significantly different among regions ($p < 0.05$; Fig. 1).
378 SSO presented the highest TEP:Chl *a* values (153.4 ± 29.8), while NSG and WA

379 presented the lowest ratios (32.3 ± 15.0 and 28.2 ± 4.8 , respectively; Fig. 1). The ratio
380 in NSO was 76.7 ± 10.6 . In the case of TEP:Phyto B and TEP:PP ratios, the SSO
381 presented the highest values and the NSG the lowest ones (Table 1).

382 TEP and POC were significantly and positively correlated across the entire transect
383 ($R^2 = 0.70$, $p < 0.001$, $n = 68$; Table 2). The contribution of TEP-C to the POC pool (TEP-
384 C%POC) ranged between 17.9 and 97.3 % (average 38.8 ± 12.3 %). TEP-C%POC in
385 the NSO and the SSO were similar (44.7 ± 6.7 and 38.5 ± 8.7 %, respectively) and
386 higher than in NSG (30.6 ± 6.2 %) and WA (25.2 ± 5.3 %; Fig. 1).

387 **3.3 TEP in relation with other variables at the sea surface**

388 TEP were significantly and positively related to Chl *a* across the entire study area ($R^2 =$
389 0.66 , $p < 0.001$, $n = 65$; Table 2) and phytoplankton biomass ($R^2 = 0.66$, $p < 0.001$, $n = 67$;
390 Table 2). The regression equation for log converted TEP vs Chl *a* was $\log \text{TEP} = 1.90$
391 $(\pm 0.02) + 0.35 (\pm 0.03) \times \log \text{Chl } a$.

392 TEP also presented significant positive relationships with temperature, salinity ($p <$
393 0.001) and all the phytoplankton groups ($p < 0.05$; Table 2), with explained variances
394 higher than 60 % for prasinophytes, dinoflagellates and diatoms. By contrast, TEP were
395 negatively related to the solar radiation dose, PHA:Chl *a*, Ddx:LHC, nutrients and wind
396 speed at the sampling time (1-h average; Table 2). TEP did not present any significant
397 relationship with PHA, although it was weakly but significantly related to PHP (Table
398 2).

399 PCA(a) and PCA(b) were performed to visualize the differences between regions and
400 the subset of variables that better explained TEP and TEP:Chl *a* patterns (Fig. 2). At
401 PCA(a) principal components 1 and 2 explained 57.1 % and 16.5 % of the variability,
402 respectively. SSO and NSG occupied the extremes of the PC1 gradient, characterized by

403 high solar radiation dose and Ddx:LHC ratio on one side (SSO) and higher TEP
404 concentrations and phytoplankton abundance, and lower macronutrient availability on
405 the other (NSG). WA and NSO showed intermediate values of PC1, but their position in
406 relationship with PC2, indicating an association with high cryptophytes and low wind
407 speed values, was opposite to that of SSO and NSG. At PCA(b), where TEP and Chl *a*
408 were replaced by TEP:Chl *a*, the regions were separated along PC1 and 2 similarly to
409 PCA(a). The major loadings to component 1 positively related to Ddx:LHC, TEP:Chl *a*
410 and solar radiation dose, and negatively related to diatoms, temperature and POC. The
411 major loadings to component 2 included cryptophytes, chlorophytes and, negatively,
412 wind speed, $F_v:F_m$ and TVA.

413 **3.4. TEP vertical distribution and relationship with other variables**

414 TEP concentrations were generally higher within the upper mixed layer (average 119.2
415 $\pm 39.0 \mu\text{g XG eq L}^{-1}$) than below it (average $53.1 \pm 45.2 \mu\text{g XG eq L}^{-1}$), and decreased
416 with depth in 4 out of 7 stations. In the other three stations, TEP maxima were found at
417 the deep Chl *a* maximum (DCM) or close to it (Fig. 3). The vertical distribution of Chl
418 *a* differed among regions, but Chl *a* concentration was generally higher in the upper 50
419 m of the water column. TEP vertical distributions were significantly related to those of
420 Chl *a* considering profiles of all regions ($R^2 = 0.74$, $p < 0.001$, $n = 26$). The equation
421 obtained for the TEP-Chl *a* vertical relationship is $\log_{10}(\text{TEP}) = 1.78 (\pm 0.04) + 0.67 (\pm$
422 $0.08) \times \log_{10}(\text{Chl } a)$. By contrast, the relationship between TEP and PHA was weak
423 ($R^2 = 0.18$, $n = 24$, $p < 0.05$). The Ddx:LHC ratio decreased strongly below 20-40 m
424 depth in all regions. TEP:Chl *a* ratios increased towards the surface in the NSO and
425 SSO, while in the other regions were constant or with the opposite pattern (Fig. S3).
426 TEP:Phyto B ratios, when available, generally followed a similar pattern than TEP:Chl
427 *a* ratios in the profiles (data not shown).

428 In NSO and WA, TEP vertical distribution was highly coupled with haptophytes and
429 cryptophytes (Fig. 3). In the NSO diatoms were higher below TEP maximum. In the
430 SSO, TEP maxima were found above or coincident with the Chl *a* peaks and always
431 above PHA maxima, and the most important phytoplankton groups (haptophytes and
432 diatoms) increased their concentration deeper in the water column (Fig. 3). In NSG, the
433 vertical TEP profile was similar to that of diatoms, which dominated the phytoplankton
434 assemblage at all depths (Fig. 3).

435 **3.5. Organic matter accumulation in the upper surface (10 cm)**

436 Among all the parameters measured in the upper surface, TEP concentration ($r= 0.71$,
437 $n= 14$), Chl *a* concentration ($r= 0.70$, $n= 13$), PHA ($r= 0.71$, $n= 13$), fucosidase ($r=0.56$,
438 $n= 14$) and esterase activity ($r= 0.82$, $n= 12$) were significantly correlated (Spearman)
439 with the measurements of the same variables at 4 m depth ($p< 0.05$).

440 At most stations, TEP and the activity of the enzymes β -glucosidase, esterase and
441 fucosidase were enriched in the upper surface (10 cm; Fig. 4) relative to 4 m. TEP- EF_{us}
442 averaged 1.19 ± 0.19 , and the EF_{us} average for the enzymatic activities were 2.75 ± 3.24
443 (β -glucosidase), 4.75 ± 1.19 (esterase) and 31.40 ± 100.78 (fucosidase). TEP- EF_{us} was
444 positively related to the 1 h-average wind speed at the time of the upper surface
445 sampling ($R^2= 0.58$, $p< 0.005$, $n= 14$) (\log_{10} transformed), which varied among 0.5 and
446 8.6 m s^{-1} , with an average of $5.4 \pm 2.5 \text{ m s}^{-1}$.

447 By contrast, Chl *a*, PHA and PHP were not usually enriched in the upper surface. Their
448 enrichment factors averaged 0.97 ± 0.37 (Chl *a*), 1.00 ± 0.27 (PHA) and 0.77 ± 0.47
449 (PHP) (Fig. 4, 7). TEP- EF_{us} and Chl *a*- EF_{us} were not significantly related ($p> 0.05$), but
450 TEP:Chl *a* ratios were generally higher at the upper surface than at the surface (average
451 TEP:Chl *a*- EF_{us} 1.37 ± 0.44).

452 **3.6. TEP variations in the 36-h cycles**

453 We did not detect recurrent diel patterns of Chl *a*, PHP or TEP in the diel cycle studies
454 (Fig. S5). TEP showed a relative amplitude (max-min/mean) of 0.31, 0.20, 0.29 and
455 0.31 in NSO, SSO, NSG and WA, respectively. Chl *a* relative amplitude (0.33, 0.07,
456 0.95 and 0.37, respectively) was highest in NSG. Looking at covariations (Spearman) of
457 TEP with other biological variables in diel cycles, TEP were only significantly ($p <$
458 0.05) coupled with Chl *a* ($r = 0.81$, $n = 8$) in NSG.

459 **3.7. TEP production by microbes during experimental incubations**

460 In the two incubation experiments (conducted in NSO and NSG), and in both treatments
461 (T and P), all measured variables (TEP, Chl *a* and PHP) increased over time, except
462 PHP in experiment NSG (Fig. 5). In the T treatments, the increases were steeper (higher
463 daily increase rates), and TEP evolved in parallel with Chl *a* concentration. The TEP
464 production rate per growth rate was 78 in the experiment NSO and 18 in the experiment
465 NSG. These values were very similar to the TEP:Chl *a* ratio average of the regions
466 where the water was collected from (76.7 ± 10.6 in the NSO and 32.5 ± 14.5 in the
467 NSG).

468

469 **4 Discussion**

470 **4.1 TEP concentrations in the Southern Ocean**

471 In the present study, we advance the existing knowledge on TEP variability across
472 environmental conditions in the Southern Ocean, with a combination of surface
473 observations, vertical profiles, short-term variability and changes associated with
474 microbial growth during laboratory incubations. The few previous studies describing
475 TEP distributions in the Southern Ocean were located around the Antarctic Peninsula

476 (Passow et al., 1995; Corzo et al., 2005; Ortega-Retuerta et al., 2009b), the Drake
477 Passage (Corzo et al., 2005) and the Ross Sea (Hong et al., 1997). Our study was carried
478 out in four distinct regions of the peninsular area, and the PCA analyses (Fig. 2)
479 confirmed a clear separation of these regions.

480 Our surface TEP concentrations are in the upper range of published values from around
481 the Antarctic Peninsula (Corzo et al., 2005; Ortega-Retuerta et al., 2009b; Table S1). In
482 contrast, the TEP:Chl *a* ratios in our study are not substantially higher than those
483 reported in previous works. It is worth mentioning that Ortega-Retuerta et al. (2009b)
484 found remarkably lower TEP and TEP:Chl *a* ratios in the western Weddell Sea area
485 compared with our SSO data (northern Weddell Sea), although the two sampling sites
486 are geographically close. Difference in the sampling periods can account for this
487 variability, since the previous study was conducted later in the season, when TEP may
488 have been consumed or degraded. The values reported by Hong et al. (1997) in the Ross
489 Sea were higher than our observations in NSO and SSO, probably because they found a
490 bloom of colonial *Phaeocystis antarctica* with higher Chl *a* concentrations and the
491 characteristic presence of mucilage flocs. Regarding vertical TEP distribution, the
492 general pattern of higher TEP concentrations in the upper mixed layer has already been
493 reported in previous studies in the SO (Hong et al., 1997; Corzo et al., 2005; Ortega-
494 Retuerta et al., 2009b) and potential causes for this pattern will be discussed below.

495 **4.2 TEP distribution and its main drivers in the Southern Ocean**

496 Phytoplankton appears to be the main driver of TEP distribution in this study at both the
497 horizontal and vertical scales, as suggested by the positive relationships between TEP
498 and Chl *a* and phytoplankton biomass. However, it is worth mentioning that the
499 coefficient of variation of surface Chl *a* concentration along the entire cruise track (81

500 %) was much higher than that of TEP (39 %). This suggested that TEP concentrations
501 were relatively more stable than those of their main sources: total phytoplankton
502 biomass expressed as Chl *a* concentration and biomass of the different phytoplankton
503 groups. Considering surface (4 m) samples only, the slope of the log-converted TEP-
504 Chl *a* relationship for the entire study ($\beta = 0.35 (\pm 0.03)$; Table 2, Fig. 6) was very
505 similar to that obtained in the Antarctic Peninsula area (Corzo et al., 2005; Ortega-
506 Retuerta et al., 2009b) but lower than those observed in the Ross Sea (Hong et al.,
507 1997), driven by the aforementioned bloom of the TEP-producing *Phaeocystis*, and in
508 the Gerlache Strait (Corzo et al., 2005). Concerning surface waters, TEP presented
509 significant positive relationships with all the phytoplankton groups. At the vertical
510 scale, the positive relationship between TEP and Chl *a* corroborates findings of previous
511 studies in the area (Corzo et al., 2005; Ortega-Retuerta et al., 2009b) and suggests that
512 phytoplankton abundance, generally higher in the upper mixed layer, is the main cause
513 for the general higher TEP concentrations found in this layer too. Our work presents for
514 the first time the vertical TEP distribution along with the phytoplankton group
515 distributions in the SO, showing that haptophytes and cryptophytes were closely
516 associated with TEP vertical distribution in the NSO and WA regions, while diatoms
517 did in the NSG region.

518 The fact that TEP:Chl *a* and TEP:Phyto B ratios were different across regions and
519 depths, further supports the role of drivers other than phytoplankton biomass on TEP
520 distribution. On this line, phytoplankton light stress appeared to control TEP
521 distributions in our study area. The SSO presented the highest solar radiation doses and
522 Ddx:LHC ratios, and the lowest $F_v:F_m$ values, which indicates stronger sunlight
523 exposure and the need for active photoacclimation (Bergmann et al., 2002; Kaiblinger et
524 al., 2007). The NSO also presented relatively high Ddx:LHC ratios and solar radiation

525 doses (Table 1). In these regions, TEP:Chl *a* ratios were the highest, which could be
526 related to a decrease of Chl *a* per cell due to photoadaptation (Kiefer et al., 1976) but
527 also to a stimulation of TEP production, as previously suggested by Iuculano et al.
528 (2017b) and Agustí and Llabrés (2007). The fact that TEP:Phyto B and TEP:PP ratios
529 were also higher in these regions than in the NSG and WA is in line with this second
530 explanation. In the PCA(b) analysis (Fig. 2), we could clearly determine that high
531 TEP:Chl *a* ratios corresponded to regions with higher macronutrient availability, solar
532 radiation dose and Ddx:LHC ratio, highlighting the role of light stress in driving
533 TEP:Chl *a* ratios.

534 The occurrence of sea ice cover and sea ice melting also seemed to influence TEP
535 concentration in the SSO region. It is known that microorganisms living in sea ice
536 release organic substances (Assmy et al., 2013; Vancoppenolle et al., 2013), including
537 TEP, as a survival strategy (Ewert and Deming, 2013). In fact, TEP concentrations
538 measured in sea ice samples during our cruise were $> 600 \mu\text{g XG eq L}^{-1}$, i.e., way above
539 concentrations in sea water, although it must be noticed that the selection of ice chunks
540 was based on their colour, picking the brownish as indicative of colonisation by algae
541 (Dall'Osto et al., 2017). The lower salinity at the surface and the larger proportion of
542 *Fragilariopsis* spp. were indicative of sea ice melt influence in SSO (Cefarelli et al.,
543 2011). Consequently, the highest TEP:Phyto B ratios in surface waters of SSO may
544 have partially resulted from an enhancement of TEP release due to sea ice melt. This
545 result agrees with previous studies suggesting sea ice melt being a source of TEP into
546 seawater (Assmy et al., 2013; Galgani et al., 2016), although this role should be studied
547 more in detail if we are to predict TEP concentrations in polar regions.

548 Nutrient depletion and the phase stage of the phytoplankton blooms could have also
549 influenced TEP distribution too, but we cannot assess this hypothesis with the data at

550 hand. NSG was the only case that presented macronutrient-deplete conditions (silicate
551 restriction; Nunes et al., 20189). The other regions probably were iron-limited, but this
552 micronutrient was not monitored. Regarding the phase stage of the phytoplankton
553 blooms, since in NSO the sea ice retreat occurred earlier in the season, we hypothesize
554 that NSO hosted an advanced phase of the SSO bloom, favoring TEP production (Corzo
555 et al., 2000). Therefore, the bloom phase as sea ice recedes, the influence of sea ice
556 melt, and the aforementioned high insolation in shallow mixed layer, all possibly
557 contributed to TEP distribution.

558 Regarding the vertical distribution, the increase of Ddx:LHC above 20-40 m in all
559 cases, indicative of protection against light stress, suggests that light stress could have
560 also triggered TEP production near surface of some regions (Iuculano et al., 2017b).
561 NSO and SSO, the regions with the strongest solar radiation doses, presented a general
562 increase of TEP:Chl *a* ratio towards the surface (Fig. S1), and also of TEP:Phyto B ratio
563 in the single profile from SSO. However, caution must be taken due to the limited data
564 available of TEP:Phyto B ratios across the profiles.

565 Heterotrophic prokaryotes did not contribute significantly to explain TEP variations
566 across the horizontal or vertical scales, given the weak relationship between TEP and
567 PHA and PHP (Table 2). Other studies have also found a lack or a negative relationship
568 between TEP and PHA or PHP (Passow and Alldredge, 1994; Bhaskar and Bhosle,
569 2006; Zamanillo et al., 2019). In contrast, some works, including two in the Southern
570 Ocean, have found a positive relationship between these variables (Passow et al., 2001;
571 Hung et al., 2003; Santschi et al., 2003; Corzo et al., 2005; Ortega-Retuerta et al.,
572 2009b; Ortega-Retuerta et al., 2010; Zamanillo et al., 2019).

573 Viral abundances did not significantly contribute to explain TEP variations neither in
574 the horizontal nor in the vertical scale (Table 2), although some studies have found a
575 link between TEP production and the viral infection of different phytoplankton taxa,
576 such as *Emiliana huxleyi* (Nissimov et al., 2018), *Phaeocystis globosa*-(Grossart et al.,
577 1998; Stoderegger and Herndl, 1999; Passow, 2002b; Brussaard et al., 2005; Mari et al.,
578 2005) and *Micromonas pusilla*-(Lønborg et al., 2013). This result suggests the
579 predominance of other factors driving TEP distribution in this study.

580 Few studies have measured and compared the distribution of TEP and other organic
581 matter compounds within the first few meters of the ocean surface (Wurl et al., 2011a;
582 Bélanger et al., 2013; Taylor et al., 2014; Thornton et al., 2016). The significant positive
583 correlations we found for most of the measured parameters (TEP, Chl *a*, PHA, esterase
584 and fucosidase activities) at 10 cm vs 4 m, indicates that the horizontal variability of
585 these parameters at the surface (4 m) is mirrored at the upper surface (10 cm). TEP were
586 generally enriched in the upper surface. The TEP-EF_{us} average (1.19 ± 0.19) was lower
587 than that found in the SML with respect to underlying water in most previous studies
588 (Wurl and Holmes, 2008; Cunliffe et al., 2009; Wurl et al., 2009; Wurl et al., 2011b;
589 Engel and Galgani, 2016; Galgani et al., 2016). This is somehow expected owing to the
590 distinct properties of the SML, which forms by the accumulation of surface-active
591 compounds (Wurl et al., 2017). However, despite the modest TEP enrichment at 10 cm,
592 TEP could be responsible for the enhancement of the activities of the ectoenzymes β -
593 glucosidase, fucosidase and esterase (Fig. 4), which are secreted by heterotrophic
594 prokaryotes to hydrolyze polysaccharides such as TEP into smaller, bio-available
595 macromolecules (Bar-Zeev and Rahav, 2015).

596 The enrichment of TEP in the upper surface was not associated with higher abundances
597 of microorganisms or higher prokaryotic heterotrophic activity (Fig. S4). Chl *a* and

598 PHA were not generally enriched in the upper surface. Therefore, reasons for the TEP
599 enrichment could be the following; (1) the increase of per-cell TEP production in the
600 upper surface due to high solar radiation (Ortega-Retuerta et al., 2009a; Iuculano et al.,
601 2017b); (2) an allochthonous source of TEP and/or their precursors at 10 cm, namely
602 sea ice melt waters of lower density; (3) ascending TEP from underlying waters,
603 embedded in low density particles or captured and transported by air bubbles (Zhou et
604 al., 1998); and (4) an increase of TEP self-assembly of dissolved precursors in the upper
605 surface due to higher turbulence (Passow, 2000; Beauvais et al., 2006). The last two
606 mechanisms are the most plausible since we found a positive relationship between TEP-
607 EF_{us} and wind speed ($R^2= 0.58$) (Fig. S4). Winds stronger than about 5 m s^{-1} cause the
608 entrainment of bubbles down from breaking waves (Andreas and Monahan, 2000;
609 Deane and Stokes, 2002), and when these bubbles rise they can bring TEP or their
610 precursors towards the surface, among other items such as prokaryotic cells (Mayol et
611 al., 2017), where aggregation is favoured by enhanced turbulence. A recent study
612 (Robinson et al., 2019) has shown that deliberate bubbling of seawater (mimicking the
613 effect of wind in the field) increases TEP concentrations in the SML, and although they
614 did not observe an increase of TEP concentration at 1 m, it is plausible that an increase
615 at 10 cm was also occurring, which is in line with our observations.

616 **4.5 TEP variations in the 36-h cycle**

617 We did not find a cyclic diel pattern of any of the measured variables (TEP, Chl *a* and
618 PHP) similarly to the outcome of the only published study on short-term TEP variation
619 (Ortega-Retuerta et al., 2017). This result illustrates the influence of many processes in
620 driving TEP distribution.

621 **4.6 TEP production by microbes in incubation experiments**

622 The results of the incubation experiments supported the idea that phytoplankton are the
623 main TEP producer in the study area (Fig. 5). In treatments with only prokaryotes, TEP
624 were formed at low rates by abiotic self-assembly and/or the action of heterotrophic
625 prokaryotes and archaea. In unfiltered treatments, TEP increased much faster and nearly
626 parallel to the Chl *a* increase. Net TEP production rates per net phytoplankton growth
627 rate varied between experiments and were very similar to the average of TEP:Chl *a*
628 ratios of the respective regions, confirming our observations that phytoplankton were
629 the main TEP producers in the study area. Interestingly, TEP production rate per
630 phytoplankton growth rate was higher in the NSO experiment than in the NSG
631 experiment, despite the higher biomass and dominance of diatoms in the latter. This
632 contradicts the common view that diatoms are highly specific TEP producers (Passow,
633 2002a), and supports the aforementioned discussed idea that environmental conditions,
634 associated physiological stress and the phytoplankton bloom stage influence TEP
635 production by phytoplankton beyond biomass, primary productivity and taxonomical
636 composition.

637

638 **5 Conclusions**

639 Our study expands the existing knowledge on TEP distribution in the Southern Ocean
640 and for the first time provides information on TEP variability in the first meters of the
641 ocean surface and with high temporal resolution. Phytoplankton abundance was the
642 main predictor of TEP distribution in both the horizontal and vertical scales, and the
643 outcome of experimental incubations further supported this observation in situ.
644 Photoacclimation and sea ice melt played complementary but important roles driving
645 differences in TEP distribution across regions. Phytoplankton composition was also an

646 important driver, especially along the vertical scale, but diatoms were not the main
647 producers. TEP were generally enriched at centimetres under the surface, likely due to
648 scavenging by bubbles and turbulence-derived aggregation, contrasting with the null
649 enrichment of microorganism abundances. We highlight the need to carry out more field
650 studies in the area, extending to temporal dynamics along the entire ice-receding and
651 ice-free season, to better predict TEP concentration in the Southern Ocean and
652 quantitatively evaluate their effects in biogeochemical processes such as the biological
653 carbon pump and organic aerosol formation.

654

655 **Author Contributions**

656 MZ conducted the study, analysed samples, processed and analysed the data. EOR and
657 RS designed the study and analysed data. SN, MEs, MS, SJR, MEm, DV, CM and DLS
658 analysed samples and provided data. MZ, EOR and RS wrote the manuscript with the
659 help of all the co-authors.

660 **Competing interests**

661 The authors declare that they have no conflict of interest

662 **Acknowledgements**

663 This research was supported by the Spanish Ministry of Economy and Competitiveness
664 through projects PEGASO (CTM2012–37615) and BIOGAPS (CTM2016–81008–R) to
665 RS. MZ was supported by a FPU predoctoral fellowship (FPU13/04630) from the
666 Spanish Ministry of Education and Culture. Gonzalo Luis Pérez, Maximino Delgado,
667 Alicia Duró, Encarna Borrull, Carolina Antequera, Clara Cardelús and Pablo
668 Rodríguez-Ros are greatly acknowledged for providing data and technical support. The

669 authors also want to thank the captain, officers and crew of RV *Hespérides*, engineers of
670 the Marine Technology Unit and researchers for their support and help during the
671 cruise.

672

673

674

675

676

677

678

679

680

681

682

683

684

685

686

687

688 **References**

689 Agustí, S., and Llabrés, M.: Solar Radiation-induced Mortality of Marine Pico-
690 phytoplankton in the Oligotrophic Ocean, *Photochemistry and Photobiology*, 83, 793-
691 801, 2007.

692 Alldredge, A. L., Passow, U., and Logan, B. E.: The abundance and significance of a
693 class of large, transparent organic particles in the ocean, *Deep Sea Research Part I:*
694 *Oceanographic Research Papers*, 40, 1131-1140, 1993.

695 Andreas, A. L., and Monahan, E. C.: The Role of Whitecap Bubbles in Air–Sea Heat
696 and Moisture Exchange, *Journal of Physical Oceanography*, 30, 433-442, 2000.

697 Assmy, P., Ehn, J. K., Fernandez-Mendez, M., Hop, H., Katlein, C., Sundfjord, A.,
698 Bluhm, K., Daase, M., Engel, A., Fransson, A., Granskog, M. A., Hudson, S. R.,
699 Kristiansen, S., Nicolaus, M., Peeken, I., Renner, A. H., Spreen, G., Tatarek, A., and
700 Wiktor, J.: Floating ice-algal aggregates below melting arctic sea ice, *PLoS One*, 8,
701 e76599, 10.1371/journal.pone.0076599, 2013.

702 Azetsu-Scott, K., and Passow, U.: Ascending marine particles: Significance of
703 transparent exopolymer particles (TEP) in the upper ocean, *Limnology and*
704 *Oceanography*, 49 741-748, 2004.

705 Bar-Zeev, E., and Rahav, E.: Microbial metabolism of transparent exopolymer particles
706 during the summer months along a eutrophic estuary system, *Front Microbiol*, 6, 403,
707 10.3389/fmicb.2015.00403, 2015.

708 Beauvais, C., Pedrotti, M. L., Egge, J., Iversen, K., and Marrasé, C.: Effects of
709 turbulence on TEP dynamics under contrasting nutrient conditions: implications for

710 aggregation and sedimentation processes, *Marine Ecology Progress Series*, 323, 47-57,
711 2006.

712 Bélanger, S., Cizmeli, S. A., Ehn, J., Matsuoka, A., Doxaran, D., Hooker, S., and Babin,
713 M.: Light absorption and partitioning in Arctic Ocean surface waters: impact of
714 multiyear ice melting, *Biogeosciences*, 10, 6433-6452, 10.5194/bg-10-6433-2013, 2013.

715 Bergmann, T., Richardson, T. L., Paerl, H. W., Pinckney, J. L., and Schofield, O.:
716 Synergy of light and nutrients on the photosynthetic efficiency of phytoplankton
717 populations from the Neuse River Estuary, North Carolina, *Journal of Plankton*
718 *Research*, 24, 923-933, 2002.

719 Bhaskar, P. V., and Bhosle, N. B.: Dynamics of transparent exopolymeric particles
720 (TEP) and particle-associated carbohydrates in the Dona Paula bay, west coast of India,
721 *Journal of Earth System Science*, 115, 403-413, 10.1007/bf02702869, 2006.

722 Boyd, P. W., and Trull, T. W.: Understanding the export of biogenic particles in oceanic
723 waters: Is there consensus?, *Progress in Oceanography*, 72, 276-312,
724 10.1016/j.pocean.2006.10.007, 2007.

725 Brussaard, C. P. D.: Optimization of Procedures for Counting Viruses by Flow
726 Cytometry, *Applied and Environmental Microbiology*, 70, 1506-1513,
727 10.1128/aem.70.3.1506-1513.2004, 2004.

728 Brussaard, C. P. D., Mari, X., Bleijswijk, J. D. L. V., and Veldhuis, M. J. W.: A
729 mesocosm study of *Phaeocystis globosa* (Prymnesiophyceae) population dynamics,
730 *Harmful Algae*, 4, 875-893, 10.1016/j.hal.2004.12.012, 2005.

731 Brussaard, C. P. D., Payet, J. P., Winter, C., and Weinbauer, M. G.: Quantification of
732 aquatic viruses by flow cytometry, in: *Manual of Aquatic Viral Ecology*, 102-109,
733 2010.

734 Buesseler, K. O.: *Ocean Biogeochemistry and the Global Carbon Cycle: An*
735 *Introduction to the U.S. Joint Global Ocean Flux Study*, 2001.

736 Burd, A. B., and Jackson, G. A.: Particle aggregation, *Ann Rev Mar Sci*, 1, 65-90,
737 10.1146/annurev.marine.010908.163904, 2009.

738 Cefarelli, A. O., Vernet, M., and Ferrario, M. E.: Phytoplankton composition and
739 abundance in relation to free-floating Antarctic icebergs, *Deep Sea Research Part II:*
740 *Topical Studies in Oceanography*, 58, 1436-1450, 10.1016/j.dsr2.2010.11.023, 2011.

741 Chin, W.-C., Orellana, M. V., and Verdugo, P.: Spontaneous assembly of marine
742 dissolved organic matter into polymer gels, *Nature*, 391, 568-572, 1998.

743 Claquin, P., Probert, I., Lefebvre, S., and Veron, B.: Effects of temperature on
744 photosynthetic parameters and TEP production in eight species of marine microalgae,
745 *Aquatic Microbial Ecology*, 51, 1-11, 10.3354/ame01187, 2008.

746 Corzo, A., Morillo, J. A., and Rodríguez, S.: Production of transparent exopolymer
747 particles (TEP) in cultures of *Chaetoceros calcitrans* under nitrogen limitation, *Aquatic*
748 *Microbial Ecology*, 23, 63-72, 10.3354/ame023063, 2000.

749 Corzo, A., Rodríguez-Gálvez, S., Lubian, L., Sangrá, P., Martínez, A., and Morillo, J.
750 A.: Spatial distribution of transparent exopolymer particles in the Bransfield Strait,
751 Antarctica, *Journal of Plankton Research*, 27, 635-646, 10.1093/plankt/fbi038, 2005.

752 Cunliffe, M., Salter, M., Mann, P. J., Whiteley, A. S., Upstill-Goddard, R. C., and
753 Murrell, J. C.: Dissolved organic carbon and bacterial populations in the gelatinous
754 surface microlayer of a Norwegian fjord mesocosm, *FEMS Microbiol Lett*, 299, 248-
755 254, 10.1111/j.1574-6968.2009.01751.x, 2009.

756 Cunliffe, M., Engel, A., Frka, S., Gašparović, B., Guitart, C., Murrell, J. C., Salter, M.,
757 Stolle, C., Upstill-Goddard, R., and Wurl, O.: Sea surface microlayers: A unified
758 physicochemical and biological perspective of the air–ocean interface, *Progress in*
759 *Oceanography*, 109, 104-116, 10.1016/j.pocean.2012.08.004, 2013.

760 Dall'Osto, M., Ovadnevaite, J., Paglione, M., Beddows, D. C. S., Ceburnis, D., Cree, C.,
761 Cortes, P., Zamanillo, M., Nunes, S. O., Perez, G. L., Ortega-Retuerta, E., Emelianov,
762 M., Vaque, D., Marrase, C., Estrada, M., Sala, M. M., Vidal, M., Fitzsimons, M. F.,
763 Beale, R., Airs, R., Rinaldi, M., Decesari, S., Cristina Facchini, M., Harrison, R. M.,
764 O'Dowd, C., and Simo, R.: Antarctic sea ice region as a source of biogenic organic
765 nitrogen in aerosols, *Sci Rep*, 7, 6047, 10.1038/s41598-017-06188-x, 2017.

766 Deane, G. B., and Stokes, M. D.: Scale dependence of bubble creation mechanisms in
767 breaking waves, *Nature*, 418, 839-844, 2002.

768 Engel, A., and Passow, U.: Carbon and nitrogen content of transparent exopolymer
769 particles (TEP) in relation to their Alcian Blue adsorption, *Marine Ecology Progress*
770 *Series*, 219, 1-10, 2001.

771 Engel, A.: Direct relationship between CO₂ uptake and transparent exopolymer particles
772 production in natural phytoplankton, *Journal of Plankton Research*, 24, 49-53, 2002.

773 Engel, A.: Distribution of transparent exopolymer particles (TEP) in the northeast
774 Atlantic Ocean and their potential significance for aggregation processes, *Deep Sea*

775 Research Part I: Oceanographic Research Papers, 51, 83-92, 10.1016/j.dsr.2003.09.001,
776 2004.

777 Engel, A., Thoms, S., Riebesell, U., Rochelle-Newall, E., and Zondervan, I.:
778 Polysaccharide aggregation as a potential sink of marine dissolved organic carbon,
779 Nature, 428, 929-932, 2004.

780 Engel, A., Borchard, C., Loginova, A., Meyer, J., Haus, H., and Kiko, R.: Effects of
781 varied nitrate and phosphate supply on polysaccharidic and proteinaceous gel particle
782 production during tropical phytoplankton bloom experiments, Biogeosciences, 12,
783 5647-5665, 10.5194/bg-12-5647-2015, 2015.

784 Engel, A., and Galgani, L.: The organic sea-surface microlayer in the upwelling region
785 off the coast of Peru and potential implications for air–sea exchange processes,
786 Biogeosciences, 13, 989-1007, 10.5194/bg-13-989-2016, 2016.

787 Ewert, M., and Deming, J. W.: Sea ice microorganisms: environmental constraints and
788 extracellular responses, Biology (Basel), 2, 603-628, 10.3390/biology2020603, 2013.

789 Frölicher, T. L., Sarmiento, J. L., Paynter, D. J., Dunne, J. P., Krasting, J. P., and
790 Winton, M.: Dominance of the Southern Ocean in Anthropogenic Carbon and Heat
791 Uptake in CMIP5 Models, Journal of Climate, 28, 862-886, 10.1175/jcli-d-14-00117.1,
792 2015.

793 Galgani, L., Piontek, J., and Engel, A.: Biopolymers form a gelatinous microlayer at the
794 air-sea interface when Arctic sea ice melts, Sci Rep, 6, 29465, 10.1038/srep29465,
795 2016.

796 Gasol, J. M., and del Giorgio, P. A.: Using flow cytometry for counting natural
797 planktonic bacteria and understanding the structure of planktonic bacterial communities,
798 *Scientia Marina*, 64, 197-224, 2000.

799 Grossart, H. P., Berman, T., Simon, M., and Pohlmann, K.: Occurrence and microbial
800 dynamics of macroscopic organic aggregates (lake snow) in Lake Kinneret, Israel, in
801 fall, *Aquatic Microbial Ecology*, 14, 59-67, 10.3354/ame014059, 1998.

802 Hansen, H. P., and Grasshoff, K.: Procedures for the automated determination of
803 seawater constituents, in: *Methods of seawater analysis*, second, revised and extended
804 edition ed., edited by: Grasshoff, K., Kremling, K., and Ehrhardt, M., Wiley, Weinheim,
805 Germany, 1983.

806 Heinonen, K. B., Ward, J. E., and Holohan, B. A.: Production of transparent
807 exopolymer particles (TEP) by benthic suspension feeders in coastal systems, *Journal of*
808 *Experimental Marine Biology and Ecology*, 341, 184-195,
809 10.1016/j.jembe.2006.09.019, 2007.

810 Higgins, H. W., Wright, S. W., and Schlüter, L.: Quantitative interpretation of
811 chemotaxonomic pigment data, *Phytoplankton Pigments*, in: *Characterization,*
812 *Chemotaxonomy and Applications in Oceanography*, edited by: Roy, S., Llewellyn, C.
813 A., Egeland, E. S., and Johnsen, G., Cambridge University Press, Cambridge, 257-313,
814 2011.

815 Hong, Y., Smith, W. O., and White, A.-M.: Studies of transparent exopolymer particles
816 (TEP) produced in the Ross Sea (Antarctica) and by *Phaeocystis antarctica*
817 (Prymnesiophyceae), *Journal of Phycology*, 33, 368 – 376, 1997.

818 Hoppe, C. J. M., Klaas, C., Ossebaar, S., Soppa, M. A., Cheah, W., Laglera, L. M.,
819 Santos-Echeandia, J., Rost, B., Wolf-Gladrow, D. A., Bracher, A., Hoppema, M.,
820 Strass, V., and Trimborn, S.: Controls of primary production in two phytoplankton
821 blooms in the Antarctic Circumpolar Current, *Deep Sea Res Part 2 Top Stud Oceanogr*,
822 138, 63-73, 10.1016/j.dsr2.2015.10.005, 2017.

823 Hung, C.-C., Guo, L., Schultz Jr, G. E., Pinckney, J. L., and Santschi, P. H.: Production
824 and flux of carbohydrate species in the Gulf of Mexico, *Global Biogeochemical Cycles*,
825 17 (2), 10.1029/2002GB001988, 2003.

826 Iuculano, F., Duarte, C. M., Marbà, N., and Augustí, S.: Seagrass as major source of
827 transparent exopolymer particles in the oligotrophic Mediterranean coast,
828 *Biogeosciences Discussions*, 1-12, 10.5194/bg-2016-558, 2017a.

829 Iuculano, F., Mazuecos, I. P., Reche, I., and Agusti, S.: *Prochlorococcus* as a Possible
830 Source for Transparent Exopolymer Particles (TEP), *Front Microbiol*, 8, 709,
831 10.3389/fmicb.2017.00709, 2017b.

832 Jenkinson, I. R., Seuront, L., Ding, H., and Elias, F.: Biological modification of
833 mechanical properties of the sea surface microlayer, influencing waves, ripples, foam
834 and air-sea fluxes, *Elem Sci Anth*, 6:26, 1-32, 10.1525/journal.elementa.283, 2018.

835 Kaiblinger, C., Greisberger, S., Teubner, K., and Dokulil, M. T.: Photosynthetic
836 efficiency as a function of thermal stratification and phytoplankton size structure in an
837 oligotrophic alpine lake, *Hydrobiologia*, 578, 29-36, 10.1007/s10750-006-0430-7, 2007.

838 Kiefer, D. A., Olson, R. J., and Holm-Hansen, O.: Another look at the nitrite and
839 chlorophyll maxima in the central North Pacific, *Deep Sea Research*, 1976.

840 Kirchman, D. L., K'Nees, E., and Hodson, R.: Leucine Incorporation and Its Potential as
841 a Measure of Protein Synthesis by Bacteria in Natural Aquatic Systems, Applied and
842 Environmental Microbiology, 49, 599-607, 1985.

843 Kuznetsova, M., Lee, C., and Aller, J.: Characterization of the proteinaceous matter in
844 marine aerosols, Marine Chemistry, 96, 359-377, 10.1016/j.marchem.2005.03.007,
845 2005.

846 Latasa, M.: A simple method to increase sensitivity for RP-HPLC phytoplankton
847 pigment analysis, Limnology and Oceanography: Methods, 12, 46-53,
848 10.4319/lom.2014.12.46, 2014.

849 Ling, S., and Alldredge, A. L.: Does the marine copepod *Calanus pacificus* consume
850 transparent exopolymer particles (TEP)?, Journal of Plankton Research, 25, 507-515,
851 2003.

852 Lønborg, C., Middelboe, M., and Brussaard, C. P. D.: Viral lysis of *Micromonas*
853 *pusilla*: impacts on dissolved organic matter production and composition,
854 Biogeochemistry, 116, 231-240, 10.1007/s10533-013-9853-1, 2013.

855 Mackey, M. D., Mackey, D. J., Higgings, H. W., and Wright, S. W.: CHEMTAX- a
856 program for estimating class abundances from chemical markers: application to HPLC
857 measurements of phytoplankton, Marine Ecology Progress Series, 144, 265-283, 1996.

858 Mari, X., and Burd, A.: Seasonal size spectra of transparent exopolymeric particles
859 (TEP) in a coastal sea and comparison with those predicted using coagulation theory,
860 1998.

861 Mari, X., Rassoulzadegan, F., Brussaard, C. P. D., and Wassmann, P.: Dynamics of
862 transparent exopolymeric particles (TEP) production by *Phaeocystis globosa* under N-
863 or P-limitation: a controlling factor of the retention/export balance, *Harmful Algae*, 4,
864 895-914, 10.1016/j.hal.2004.12.014, 2005.

865 Mari, X., Passow, U., Migon, C., Burd, A. B., and Legendre, L.: Transparent
866 exopolymer particles: Effects on carbon cycling in the ocean, *Progress in*
867 *Oceanography*, 151, 13-37, 10.1016/j.pocean.2016.11.002, 2017.

868 Marinov, I., Gnanadesikan, A., Sarmiento, J. L., Toggweiler, J. R., Follows, M., and
869 Mignone, B. K.: Impact of oceanic circulation on biological carbon storage in the ocean
870 and atmospheric $p\text{CO}_2$, *Global Biogeochemical Cycles*, 22, 1-15,
871 10.1029/2007gb002958, 2008.

872 Mayol, E., Arrieta, J. M., Jimenez, M. A., Martinez-Asensio, A., Garcias-Bonet, N.,
873 Dachs, J., Gonzalez-Gaya, B., Royer, S. J., Benitez-Barrios, V. M., Fraile-Nuez, E., and
874 Duarte, C. M.: Long-range transport of airborne microbes over the global tropical and
875 subtropical ocean, *Nat Commun*, 8, 201, 10.1038/s41467-017-00110-9, 2017.

876 Menden-Deuer, S., and Lessard, E. J.: Carbon to volume relationships for
877 dinoflagellates, diatoms, and other protist plankton, *Limnology and Oceanography*, 45,
878 569-579, 2000.

879 Monterey, G., and Levitus, S.: Seasonal variability of mixed layer depth for the world
880 ocean, NOAA ATLAS, NESDIS, 14, 96 pp, 1997.

881 Moore, C. M., Mills, M. M., Arrigo, K. R., Berman-Frank, I., Bopp, L., Boyd, P. W.,
882 Galbraith, E. D., Geider, R. J., Guieu, C., Jaccard, S. L., Jickells, T. D., La Roche, J.,
883 Lenton, T. M., Mahowald, N. M., Marañón, E., Marinov, I., Moore, J. K., Nakatsuka,

884 T., Oschlies, A., Saito, M. A., Thingstad, T. F., Tsuda, A., and Ulloa, O.: Processes and
885 patterns of oceanic nutrient limitation, *Nature Geoscience*, 6, 701-710,
886 10.1038/ngeo1765, 2013.

887 Morris, P. J., and Sanders, R.: A carbon budget for a naturally iron fertilized bloom in
888 the Southern Ocean, *Global Biogeochemical Cycles*, 25, n/a-n/a,
889 10.1029/2010gb003780, 2011.

890 Mueller, J. L., Morel, A., Frouin, R., Davis, C. O., Arnone, R. A., Carder, K. L., Lee,
891 Z., Steward, R. G., Hooker, S. B., Mobley, C. D., McLean, S., Holben, B. N., Miller,
892 M., Pietras, C., Knobelspiesse, K. D., Fargion, G. S., Porter, J., and Voss, J. L.: Ocean
893 optics protocols for satellite ocean color sensor validation, revision 4, volume III:
894 radiometric measurements and data analysis protocols. , *Ocean Opt. Protoc. Satell.*
895 *Ocean Color Sens*, 4 (III), 78, 2003.

896 Nicolaus, B., Panico, A., Lama, L., Romano, I., Manca, M. C., De Giulio, A., and
897 Gambacorta, A.: Chemical composition and production of exopolysaccharides from
898 representative members of heterocystous and non-heterocystous cyanobacteria,
899 *Phytochemistry*, 52, 639-647, 1999.

900 Nissimov, J. I., Vandzura, R., Johns, C. T., Natale, F., Haramaty, L., and Bidle, K. D.:
901 Dynamics of transparent exopolymer particle production and aggregation during viral
902 infection of the coccolithophore, *Emiliana huxleyi*, *Environ Microbiol*, 20, 2880-2897,
903 10.1111/1462-2920.14261, 2018.

904 Nunes, S., Latasa, M., Delgado, M., Emelianov, M., Simó, R., and Estrada, M.:
905 Phytoplankton community structure in contrasting ecosystems of the Southern Ocean:

906 South Georgia, South Orkneys and Western Antarctic Peninsula, Deep Sea Res I (under
907 review), 2019.

908 Orellana, M. V., and Verdugo, P.: Ultraviolet radiation blocks the organic carbon
909 exchange between the dissolved phase and the gel phase in the ocean, *Limnology and*
910 *Oceanography*, 48 (4), 1618-1623, 2003.

911 Ortega-Retuerta, E., Passow, U., Duarte, C. M., and Reche, I.: Effects of ultraviolet B
912 radiation on (not so) transparent exopolymer particles, *Biogeosciences*, 6, 3071-3080,
913 10.5194/bg-6-3071-2009, 2009a.

914 Ortega-Retuerta, E., Reche, I., Pulido-Villena, E., Agustí, S., and Duarte, C. M.:
915 Uncoupled distributions of transparent exopolymer particles (TEP) and dissolved
916 carbohydrates in the Southern Ocean, *Marine Chemistry*, 115, 59-65,
917 10.1016/j.marchem.2009.06.004, 2009b.

918 Ortega-Retuerta, E., Duarte, C. M., and Reche, I.: Significance of bacterial activity for
919 the distribution and dynamics of transparent exopolymer particles in the Mediterranean
920 sea, *Microb Ecol*, 59, 808-818, 10.1007/s00248-010-9640-7, 2010.

921 Ortega-Retuerta, E., Sala, M. M., Borrull, E., Mestre, M., Aparicio, F. L., Gallisai, R.,
922 Antequera, C., Marrase, C., Peters, F., Simo, R., and Gasol, J. M.: Horizontal and
923 Vertical Distributions of Transparent Exopolymer Particles (TEP) in the NW
924 Mediterranean Sea Are Linked to Chlorophyll *a* and O₂ Variability, *Front Microbiol*, 7,
925 2159, 10.3389/fmicb.2016.02159, 2017.

926 Passow, U., and Alldredge, A. L.: Distribution, size and bacterial colonization of
927 transparent exopolymer particles (TEP) in the ocean, *Marine Ecology Progress Series*,
928 113, 185-198, 1994.

929 Passow, U., Alldredge, A. L., and Logan, B. E.: The role of particulate carbohydrate
930 exudates in the flocculation of diatom blooms, *Deep-Sea Res. I Oceanogr. Res.*, 41,
931 335-357, 1994.

932 Passow, U., and Alldredge, A. L.: A dye-binding assay for the spectrophotometric
933 measurement of transparent exopolymer particles (TEP), *Limnology and Oceanography*,
934 40, 1326-1335, 1995.

935 Passow, U., Kozłowski, W., and Vernet, M.: Palmer LTER: Temporal variability of
936 transparent exopolymer particles in Arthur Harbor during the 1994-1995 growth season,
937 *Antarctic Journal-Review*, 265-266, 1995.

938 Passow, U.: Formation of transparent exopolymer particles, TEP, from dissolved
939 precursor material, *Marine Ecology Progress Series*, 192, 1-11, 2000.

940 Passow, U., Shipe, R. F., Murray, A., Pak, D. K., Brzezinski, M. A., and Alldredge, A.
941 L.: The origin of transparent exopolymer particles (TEP) and their role in the
942 sedimentation of particulate matter, *Continental Shelf Research*, 21, 327-346, 2001.

943 Passow, U.: Production of transparent exopolymer particles (TEP) by phyto- and
944 bacterioplankton, *Marine Ecology Progress Series*, 236, 1-12, 2002a.

945 Passow, U.: Transparent exopolymer particles (TEP) in aquatic environments, *Progress*
946 *in Oceanography*, 55, 287-333, 2002b.

947 Pedrotti, M. L., Peters, F., Beauvais, S., Vidal, M., Egge, J., Jacobsen, A., and Marrasé,
948 C.: Effects of nutrients and turbulence on the production of transparent exopolymer
949 particles: a mesocosm study, *Marine Ecology Progress Series*, 419, 57-69,
950 10.3354/meps08840, 2010.

951 Prieto, L., Sommer, F., Stibor, H., and Koeve, W.: Effects of planktonic copepods on
952 transparent exopolymeric particles (TEP) abundance and size spectra, *Journal of*
953 *Plankton Research*, 5, 515-525, 2001.

954 Robinson, T. B., Wurl, O., Bahlmann, E., Jürgens, K., and Stolle, C.: Rising bubbles
955 enhance the gelatinous nature of the air–sea interface, *Limnology and Oceanography*,
956 10.1002/lno.11188, 2019.

957 Royer, S. J., Mahajan, A. S., Galí, M., Saltzman, E., and Simó, R.: Small-scale
958 variability patterns of DMS and phytoplankton in surface waters of the tropical and
959 subtropical Atlantic, Indian, and Pacific Oceans, *Geophysical Research Letters*, 42, 475-
960 483, 10.1002/2014gl062543, 2015.

961 Sala, M. M., Aparicio, F. L., Balagué, V., Boras, J. A., Borrull, E., Cardelús, C., Cros,
962 L., Gomes, A., López-Sanz, A., Malits, A., Martínez, R. A., Mestre, M., Movilla, J.,
963 Sarmiento, H., Vázquez-Domínguez, E., Vaqué, D., Pinhassi, J., Calbet, A., Calvo, E.,
964 Gasol, J. M., Pelejero, C., and Marrasé, C.: Contrasting effects of ocean acidification on
965 the microbial food web under different trophic conditions, *ICES Journal of Marine*
966 *Science: Journal du Conseil*, 73, 670-679, 10.1093/icesjms/fsv130, 2016.

967 Santschi, P. H., Hung, C.-C., Schultz, G., and Alvarado-Quiroz, N.: Control of acid
968 polysaccharide production and ²³⁴Th and POC export fluxes by marine organisms,
969 *Geophysical Research Letters*, 30 (2), 10.1029/2002GL016046, 2003.

970 Sarmiento, J. L., Gruber, N., Brzezinski, M. A., and Dunne, J. P.: High-latitude controls
971 of thermocline nutrients and low latitude biological productivity, *Nature*, 427, 56-60,
972 2004.

973 Schlitzer, R., 2017. Ocean Data View. <http://odv.awi.de>.

974 Shammi, M., Pan, X., Mostofa, K. M. G., Zhang, D., and Liu, C. Q.: Photo-flocculation
975 of microbial mat extracellular polymeric substances and their transformation into
976 transparent exopolymer particles: Chemical and spectroscopic evidences, *Sci Rep*, 7,
977 9074, 10.1038/s41598-017-09066-8, 2017.

978 Simó, R., Vila-Costa, M., Alonso-Sáez, L., Cardelús, C., Guadayol, Ò., Vázquez-
979 Domínguez, E., and Gasol, J. M.: Annual DMSP contribution to S and C fluxes through
980 phytoplankton and bacterioplankton in a NW Mediterranean coastal site, *Aquatic*
981 *Microbial Ecology*, 57, 43-55, 10.3354/ame01325, 2009.

982 Smith, D. C., and Azam, F.: A simple, economical method for measuring bacterial
983 protein synthesis rates in seawater using ^3H -leucine *Marine Microbial Food Web*, 6 (2),
984 107-114, 1992.

985 Steeman-Nielsen, E.: The Use of Radio-active Carbon (C^{14}) for Measuring Organic
986 Production in the Sea, *ICES Journal of Marine Science*, 18, 117-140, 1952.

987 Stoderegger, K., and Herndl, G. J.: Production of exopolymer particles by marine
988 bacterioplankton under contrasting turbulence conditions, *Marine Ecology Progress*
989 *Series*, 189, 9-16, 1999.

990 Taylor, J. D., Cottingham, S. D., Billinge, J., and Cunliffe, M.: Seasonal microbial
991 community dynamics correlate with phytoplankton-derived polysaccharides in surface
992 coastal waters, *ISME J*, 8, 245-248, 10.1038/ismej.2013.178, 2014.

993 Thornton, D. C. O., Brooks, S. D., and Chen, J.: Protein and Carbohydrate Exopolymer
994 Particles in the Sea Surface Microlayer (SML), *Frontiers in Marine Science*, 3,
995 10.3389/fmars.2016.00135, 2016.

996 Utermöhl, H.: Zur Vervollkommnung der quantitativen Phytoplankton-Methodik,
997 Mitteilungen der International Vereinigung für theoretische und Angewandte
998 Limnologie, 9, 1-38, 1958.

999 Van Oostende, N., Harlay, J., Vanellander, B., Chou, L., Vyverman, W., and Sabbe,
1000 K.: Phytoplankton community dynamics during late spring coccolithophore blooms at
1001 the continental margin of the Celtic Sea (North East Atlantic, 2006–2008), Progress in
1002 Oceanography, 104, 1-16, 10.1016/j.pocean.2012.04.016, 2012.

1003 Vancoppenolle, M., Meiners, K. M., Michel, C., Bopp, L., Brabant, F., Carnat, G.,
1004 Delille, B., Lannuzel, D., Madec, G., Moreau, S., Tison, J.-L., and van der Merwe, P.:
1005 Role of sea ice in global biogeochemical cycles: emerging views and challenges,
1006 Quaternary Science Reviews, 79, 207-230, 10.1016/j.quascirev.2013.04.011, 2013.

1007 Wurl, O., and Holmes, M.: The gelatinous nature of the sea-surface microlayer, Marine
1008 Chemistry, 110, 89-97, 10.1016/j.marchem.2008.02.009, 2008.

1009 Wurl, O., Miller, L., Röttgers, R., and Vagle, S.: The distribution and fate of surface-
1010 active substances in the sea-surface microlayer and water column, Marine Chemistry,
1011 115, 1-9, 10.1016/j.marchem.2009.04.007, 2009.

1012 Wurl, O., Miller, L., and Vagle, S.: Production and fate of transparent exopolymer
1013 particles in the ocean, Journal of Geophysical Research, 116, 10.1029/2011jc007342,
1014 2011a.

1015 Wurl, O., Wurl, E., Miller, L., Johnson, K., and Vagle, S.: Formation and global
1016 distribution of sea-surface microlayers, Biogeosciences, 8, 121-135, 10.5194/bg-8-121-
1017 2011, 2011b.

1018 Wurl, O., Stolle, C., Van Thuoc, C., The Thu, P., and Mari, X.: Biofilm-like properties
1019 of the sea surface and predicted effects on air–sea CO₂ exchange, *Progress in*
1020 *Oceanography*, 144, 15-24, 10.1016/j.pocean.2016.03.002, 2016.

1021 Wurl, O., Ekau, W., Landing, W. M., and Zappa, C. J.: Sea surface microlayer in a
1022 changing ocean – A perspective, *Elem Sci Anth*, 5, 10.1525/elementa.228, 2017.

1023 Yentsch, C. S., and Menzel, D. W.: A method for the determination of phytoplankton
1024 chlorophyll and phaeophytin by fluorescence, *Deep Sea Res I*, 10, 221-231, 1963.

1025 Zamanillo, M., Ortega-Retuerta, E., Nunes, S., Rodríguez-Ros, P., Dall'Osto, M.,
1026 Estrada, M., Sala, M. M., and Simó, R.: Main drivers of transparent exopolymer particle
1027 distribution across the surface Atlantic Ocean, *Biogeosciences*, 16, 733-749,
1028 10.5194/bg-16-733-2019, 2019.

1029 Zhou, J., Mopper, K., and Passow, U.: The role of surface-active carbohydrates in the
1030 formation of transparent exopolymer particles by bubble adsorption of seawater,
1031 *Limnology and Oceanography*, 43, 1860-1871, 1998.

1032 **Figure captions**

1033 **Figure 1:** Boxplots of transparent exopolymer particles (TEP), chlorophyll *a* (Chl *a*),
1034 TEP:Chl *a*, contribution of TEP-C to the POC (particulate organic carbon) pool (TEP-
1035 C%POC), solar radiation dose, Ddx:LHC ratio (Ddx: Diadinoxanthin, LHC: sum of the
1036 main light-harvesting carotenoids), prokaryotic heterotrophic abundance (PHA) and
1037 prokaryotic heterotrophic production (PHP) in the surface of the four visited regions
1038 :North of the South Orkney Islands (NSO), South of the South Orkney Islands (SSO),
1039 Northwest of South Georgia Island (NSG), West of Anvers Island (WA). The
1040 horizontal lines of the boxes represent 25%, 50% (median) and 75% percentiles (from
1041 bottom to top). Whiskers represent minimum and maximum values.

1042
1043 **Figure 2:** Principal component analyses (PCA) of surface (4 m) samples. The % of the
1044 overall explained variance is given on each principal component axis. The plot (b) is the
1045 same as (a) plot after replacing transparent exopolymer particles (TEP) and chlorophyll
1046 *a* (Chl *a*) by TEP:Chl *a*. Note that the opposite direction of axes in PCA(a) and (b) is
1047 only due to calculations Chlorophytes (Chlor), cryptophytes (Crypt), diatoms (Diat),
1048 dinoflagellates (Dinof), haptophytes (Hapt), prasinophytes (Pras), pelagophytes
1049 (Pelago), Ddx:LHC (see Fig. 1 for abbreviations), Maximum quantum efficiency of
1050 photosystem II photochemistry (FvFm), temperature (Temp), total viral abundance
1051 (TVA), prokaryotic heterotrophic production (PHP) and particulate organic carbon
1052 (POC).

1053 **Figure 3:** Vertical profiles of temperature (Temp), salinity (Sal), concentration of the
1054 different phytoplankton groups derived from CHEMTAX (see Fig. 2 for abbreviations),
1055 transparent exopolymer particles (TEP), chlorophyll *a* (Chl *a*) and prokaryotic
1056 heterotrophic abundance (PHA) in every region (see Fig. 1 for abbreviations of regions).

1057 **Figure 4:** Boxplots of EF_{us} of transparent exopolymer particles (TEP), chlorophyll *a*
1058 (Chl *a*), TEP:Chl *a*, prokaryotic heterotrophic abundance (PHA), prokaryotic
1059 heterotrophic production (PHP), and fucosidase, esterase and β -glucosidase activities
1060 across the study regions ($n = 14$). See Fig. S4 for the definition of EF_{us} .

1061 **Figure 5:** Incubation experiments at NSO (top) and NSG (bottom). Transparent
1062 exopolymer particles (TEP) concentration (blue circle), prokaryotic heterotrophic
1063 production (PHP) (pink triangle) and chlorophyll *a* (Chl *a*) (green square) are plotted
1064 over time (h). Filled symbols and continuous lines: unfiltered water (treatment T).
1065 Empty symbols and dashed lines: water filtered through $0.8 \mu\text{m}$, hence, only with
1066 prokaryotes (treatment P).

1067
1068 **Figure 6:** Log-log relationship between transparent exopolymer particles (TEP) and
1069 chlorophyll *a* (Chl *a*) concentration from the PEGASO cruise, with the linear regression
1070 line (regression equation in the text). Four regions are distinguished: NSO (empty
1071 circles), SSO (empty triangles), NSG (filled circles), WA (crosses) (see Fig. 1 for
1072 abbreviations of regions), T: transect (plus). Regression lines from the literature in the
1073 Southern Ocean are also shown for comparison. α and β indicate the intercept and the
1074 slope, respectively; $\log \text{TEP} (\mu\text{g XG eq L}^{-1}) = \alpha + \beta \times \log \text{Chl } a (\mu\text{g L}^{-1})$; [a] $\alpha = 2.25$
1075 and $\beta = 0.65$, (Hong et al., 1997); [b] $\alpha = 1.63$ and $\beta = 0.32$, (Corzo et al., 2005); [c] $\alpha =$

1076 1.52 and $\beta = 0.67$, (Corzo et al., 2005); [d] $\alpha = 1.08$ and $\beta = 0.38$, (Ortega–Retuerta et
1077 al., 2009b).

1078

1079 **Figure S1:** Study area. Ship trajectory (blue line) and the four case studies with
1080 Lagrangian occupation (circles, see Fig. 1 for abbreviations of regions). Main
1081 hydrographic fronts (black lines) along the cruise: Antarctic Polar Front (PF), Southern
1082 Antarctic Circumpolar Current Front (SACCF), Southern Boundary of the Antarctic
1083 Circumpolar Current (SB), and Weddell Scotia Confluence Zone (WSCF). Figure
1084 produced with the Ocean Data View software.

1085

1086 **Figure S2:** Average concentration of each phytoplankton group in the sea surface of the
1087 four visited regions derived from CHEMTAX (contribution to the total Chl *a*, ng Chl *a*
1088 L⁻¹) (see Fig. 1 for abbreviations of regions).

1089 **Figure S3:** Vertical profiles of TEP:Chl *a* ratio (transparent exopolymer particles
1090 (TEP), chlorophyll *a* (Chl *a*)) in every study region (see Fig. 1 for abbreviations of
1091 regions).

1092

1093 **Figure S4:** Enrichment factor between the upper surface (10 cm) and the surface (4 m)
1094 ($EF_{us} = [X]_{\text{upper surface}} / [X]_{\text{surface}}$) for transparent exopolymer particles (TEP),
1095 chlorophyll *a* (Chl *a*), prokaryotic heterotrophic abundance (PHA) and prokaryotic
1096 heterotrophic production (PHP) (bars) in the different regions (see Fig. 1 for
1097 abbreviations of regions). Horizontal line denotes $EF_{us} = 1$. Wind speed is indicated by
1098 filled circles. T: transect.

1099

1100 **Figure S5:** Transparent exopolymer particles (TEP) concentration (blue circle),
1101 prokaryotic heterotrophic production (PHP) (pink triangle) and chlorophyll *a* (Chl *a*)
1102 (green square) in the 36-h cycles (local time, UTC-3) in every visited region (see Fig. 1
1103 for abbreviations of regions). Grey shaded areas indicate night by enclosing the period
1104 when global solar radiation was $< 10 \text{ W m}^{-2}$.

1105

Table 1. Mean \pm standard deviation of several variables and dominant phytoplankton groups in the sea surface (4 m depth) of the four study regions. MLD: mixed layer depth. Phyto B: Phytoplankton biomass. PP: Primary production. POC: Particulate organic carbon. PHA and PHP: Prokaryote heterotrophic abundance and production, respectively. TVA and LVA: Total and large viral abundance, respectively. $F_v:F_m$: Maximum quantum efficiency of photosystem II photochemistry. Ddx:LHC: Ddx, diadinoxanthin; LHC, sum of the main light-harvesting carotenoids. TEP: Transparent exopolymer particles. See Fig. 1 for abbreviations of regions.

	NSO (n= 16)	SSO (n= 15)	NSG (n= 14)	WA (n= 9)
Date (d/m/y)	10-15/01/2015	16-20/01/2015	23-25/01/2015	02-03/02/2015
Temperature ($^{\circ}\text{C}$)	0.59 ± 0.15^a	-0.75 ± 0.11^b	4.77 ± 0.45^c	1.46 ± 0.09^d
Salinity	33.83 ± 0.08^a	33.15 ± 0.05^b	33.74 ± 0.02^c	33.41 ± 0.03^d
MLD (m)	28.9 ± 11.8^a	15.8 ± 5.4^b	49.3 ± 11.8^c	22.9 ± 5.6^{ab}
Ice cover (%)	0^e	> 25	0	0
Solar radiation dose (W m^{-2})	80.3 ± 40.4^a	101.7 ± 20.3^a	22.4 ± 5.4^b	47.0 ± 10.6^b
Nitrate ($\mu\text{mol L}^{-1}$)	27.3 ± 1.9^a	27.5 ± 3.2^a	17.2 ± 1.6^b	18.7 ± 0.9^b
Phosphate ($\mu\text{mol L}^{-1}$)	2.0 ± 0.2^{aa}	2.1 ± 0.3^{ab}	1.3 ± 0.2^c	1.8 ± 0.2^{aa}
Silicate ($\mu\text{mol L}^{-1}$)	47.9 ± 4.1^a	47.3 ± 4.7^a	2.0 ± 0.4^b	49.7 ± 3.7^a
Chl <i>a</i> ($\mu\text{g L}^{-1}$)	1.87 ± 0.23^a	0.32 ± 0.06^b	4.59 ± 1.97^c	4.05 ± 0.48^c
Phyto B ($\mu\text{g C L}^{-1}$)	95.7 ± 21.0^a	22.3 ± 4.4^b	222.1 ± 53.1^c	94.4 ± 37.5^a
PP ($\text{mg C m}^{-3} \text{d}^{-1}$)	13.0 ± 4.0^a	3.7 ± 0.8^a	111.6 ± 85.4^b	34.6 ± 15.7^a
POC ($\mu\text{mol L}^{-1}$)	13.8 ± 2.6^a	5.5 ± 1.2^b	18.0 ± 4.4^c	19.3 ± 3.5^c
PHA ($\text{cells mL}^{-1} \times 10^5$)	2.34 ± 0.46^a	2.89 ± 0.70^{ab}	5.68 ± 0.98^c	3.43 ± 0.95^b
PHP ($\mu\text{g C L}^{-1} \text{d}^{-1}$)	0.50 ± 0.16^a	0.32 ± 0.19^a	1.23 ± 0.66^b	0.40 ± 0.14^a
TVA ($\text{virus mL}^{-1} \times 10^5$)	44.8 ± 21.8^a	32.3 ± 17.1^a	211.2 ± 99.8^b	137.1 ± 42.5^c
LVA ($\text{virus mL}^{-1} \times 10^5$)	2.8 ± 0.9^a	2.5 ± 2.3^a	25.3 ± 19.5^b	8.9 ± 5.1^a
Dominant phytoplankton groups	Cryptophytes > haptophytes > diatoms	Haptophytes > cryptophytes ~ chlorophytes ~ diatoms	Diatoms	Cryptophytes >> haptophytes > diatoms
$F_v:F_m$	0.18 ± 0.06^a	0.16 ± 0.05^a	0.29 ± 0.05^b	0.21 ± 0.06^a
Ddx:LHC	0.36 ± 0.06^a	0.58 ± 0.09^b	0.19 ± 0.04^c	0.25 ± 0.04^c
TEP ($\mu\text{g XG eq L}^{-1}$)	144.4 ± 21.7^a	48.1 ± 6.5^b	125.5 ± 21.1^c	111.6 ± 13.0^c
TEP:Chl <i>a</i> ($\mu\text{g XG eq } \mu\text{g}^{-1}$)	76.7 ± 10.6^a	153.4 ± 29.8^b	32.3 ± 15.0^c	28.2 ± 4.8^c

TEP:Phyto B	1.56 ± 0.35 ^a	2.24 ± 0.54 ^b	0.61 ± 0.18 ^c	1.26 ± 0.36 ^a
TEP:PP	12.5 ± 3.1 ^{a,b}	14.0 ± 5.7 ^a	1.8 ± 1.3 ^c	4.6 ± 4.1 ^{b,c}
TEP:POC (µg XG µg C ⁻¹)	0.9 ± 0.1 ^a	0.8 ± 0.2 ^a	0.6 ± 0.1 ^b	0.5 ± 0.1 ^b

^{a, b, c, d} significantly different (p < 0.05) groups using non-parametric ANOVA followed by post-hoc tests (Tukey).

^e ice cover was > 25 % two months before our study

Table 2. Regression equations and statistics describing the relationship between transparent exopolymer particles (TEP) (dependent variable) and several independent variables across surface samples in the entire PEGASO cruise (note all variables were \log_{10} -transformed). Regressions with $p < 0.05$ are highlighted. PVA: phage viral abundance. See Table 1 for abbreviations.

Dep. var.	Independent var.	R ²	p	Intercept	Slope	n
TEP	Temperature ^a	0.27	< 0.001	-78.1	32.8	66
	Salinity	0.25	< 0.001	-33.74	23.38	66
	Wind speed	0.08	< 0.05	2.13	-0.19	67
	Nitrate	0.10	< 0.05	2.84	-0.63	69
	Phosphate	0.14	< 0.05	2.18	-0.77	69
	Silicate	0.06	< 0.05	2.08	-0.08	69
	Solar radiation dose	0.24	< 0.001	2.65	-0.38	46
	Chl <i>a</i>	0.66	< 0.001	1.90	0.35	65
	Phyto B	0.66	< 0.001	1.17	0.43	67
	PP	0.43	< 0.05	1.67	0.25	19
	PHA	0.01	> 0.05			71
	PHP	0.18	< 0.001	2.07	0.25	68
	TVA	0.16	< 0.001	0.45	0.22	71
	LVA	0.08	< 0.05	1.27	0.12	71
	PVA	0.18	< 0.001	0.41	0.23	71
	POC ^b	0.70	< 0.001	-1.00	1.03	68
	PHA:Chl <i>a</i>	0.71	< 0.001	4.07	-0.39	64
	F _v :F _m	0.04	> 0.05			71
	Ddx:LHC	0.18	< 0.001	1.74	-0.42	68
	Prasinophytes ^c	0.68	< 0.001	1.86	0.14	37
	Chlorophytes ^c	0.17	< 0.05	1.72	0.23	38
	Dinoflagellates ^c	0.67	< 0.001	1.57	0.32	38
	Cryptophytes ^c	0.47	< 0.001	1.65	0.18	38
	Diatoms ^c	0.67	< 0.001	1.62	0.18	38
	Pelagophytes ^c	0.58	< 0.001	1.83	0.15	38

Haptophytes ^c	0.52	< 0.001	0.78	0.51	38
--------------------------	-------------	-------------------	-------------	-------------	----

R²: explained variance; sample size; p: level of significance; n: sample size

^a Kelvin degrees, ^b POC as dependent variable, ^c ng Chl *a* L⁻¹

Table S1. Compilation of published transparent exopolymer particles (TEP) concentrations (mean \pm SE and ranges; $\mu\text{g XG eq L}^{-1}$), chlorophyll *a* (Chl *a*) concentrations (mean \pm SE and ranges; $\mu\text{g L}^{-1}$) and TEP:Chl *a* ratios (mean \pm SE and ranges; $\mu\text{g XG eq } (\mu\text{g Chl } a)^{-1}$) in the Southern Ocean. Bdl: below detection limit.

Location	Comments	TEP	Chl <i>a</i>	TEP:Chl <i>a</i>	Reference
Anvers Island	Summer (November 1994-February 1995) 2- 6 m, coastal samples Two blooms observed (Cryptomonads and diatoms)	15 - >500	-	-	Passow et al. (1995)
Kita-no-seto Strait	Mid-January 1994 15 m	26 \pm6-41\pm4 particles mL ⁻¹	-	-	Marchant et al. (1996)
Ross Sea	Summer (November, December 1994) 0-150 m, <i>Phaeocystis</i> and diatoms bloom	Surface 308 (0-2800)	3.61 (0.27-8.81) (surface)	89.1 (surface)	Hong et al. (1997)
Bransfield Strait	Summer (13 December 1990- 3	56.77 \pm 54.50 (bdl-345.9)	0.98 \pm 0.83 (0.05-4.81)	51.0	Corzo et al. (2005)
Gerlache Strait	January 2000)	38 (0-283)	1.16	32.7	
Drake Passage	0-100 m	35 (0-157)	1.17	29.9	
Antarctic Peninsula (all the study)	Summer (February 2005), 0-200 m	15.4 \pm 10.0 (bdl-48.9)	0.01-5.36	40.9 \pm 157.8 (bdl-1492)	Ortega-Retuerta et al. (2009b)
Bellingshausen Sea		14.3 \pm 9.5 (bdl-33.8)		84.2 \pm 257.5 (bdl-1492)	
Weddell Sea		16.3 \pm 12.5 (bdl-48.9)		9.8 \pm 7.4 (1.2-28.4)	
Bransfield and Gerlache Strait		15.8 \pm 8.9 (bdl-35.8)		15.0 \pm 20.4 (3.0-18.0)	
Southern Ocean (all transect)	Summer (7 January-3 February 2015) 4 m	102.3 \pm 40.4 (39.2- 177.6)	2.36 \pm 1.92 (0.28-8.95)	79.3 \pm 54.9 (10.9-239.0)	This study
South Orkney Islands (NSO)		144.4 \pm 21.7 (97.8-177.6)	1.87 \pm 0.23 (1.58-2.21)	76.7 \pm 10.6 (60.4-97.5)	
southeast of the South Orkney Islands (SSO)		48.1 \pm 6.5 (39.2-63.8)	0.32 \pm 0.06 (0.28-0.45)	153.4 \pm 29.8 (102.5-211.6)	
northwest of South Georgia (NSG)		125.5 \pm 21.1 (93.6-157.4)	4.59 \pm 1.97 (1.92-8.95)	32.3 \pm 15.0 (17.6-70.0)	
west of Anvers Island (WA)		111.6 \pm 13.0 (90.5-125.0)	4.05 \pm 0.48 (3.41-4.91)	28.2 \pm 4.8 (18.4-34.9)	

Figure 1

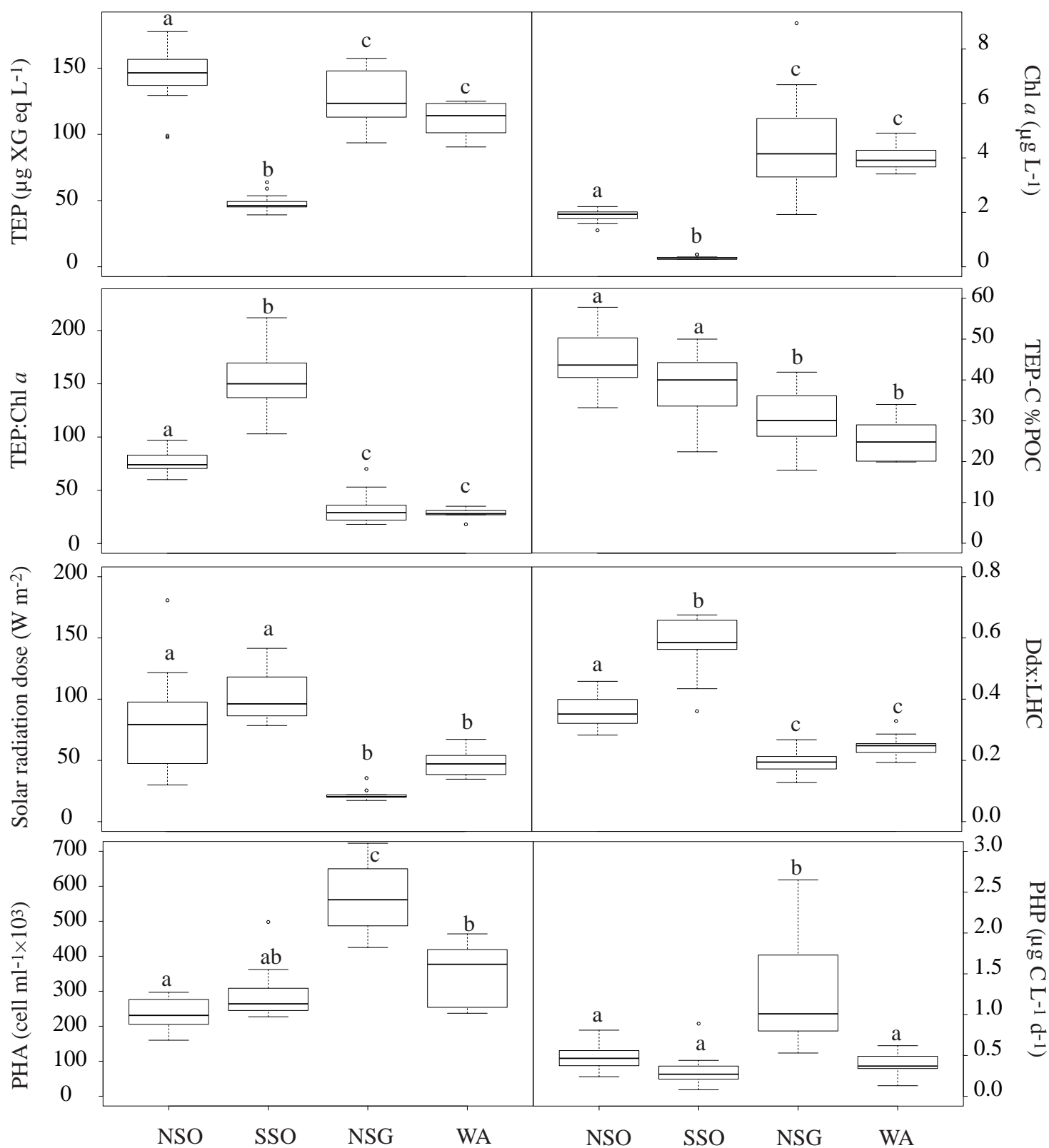
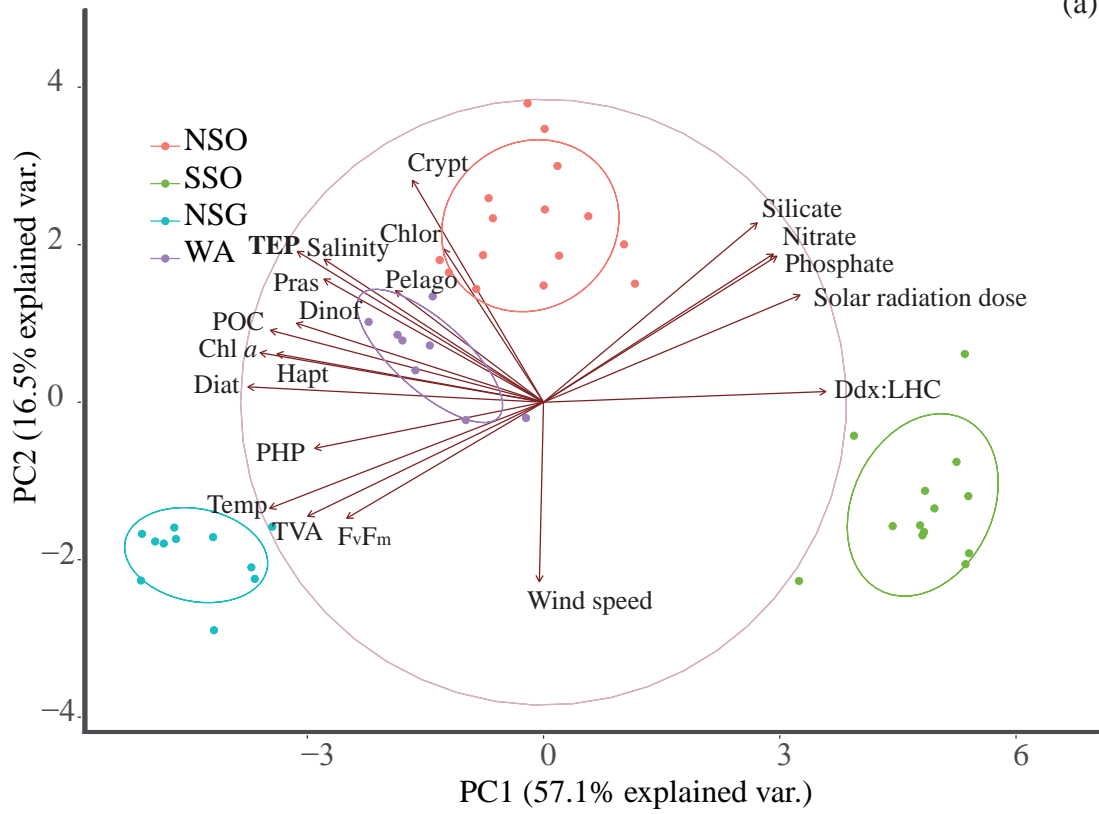


Figure 2

(a)



(b)

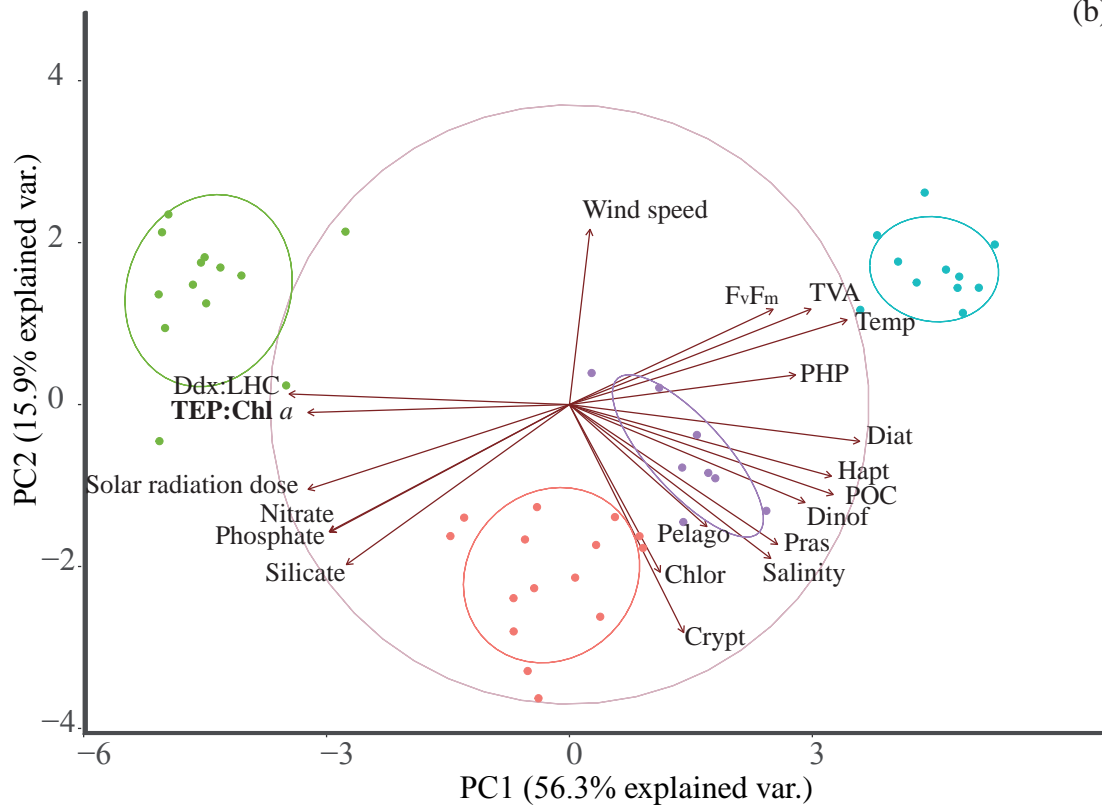
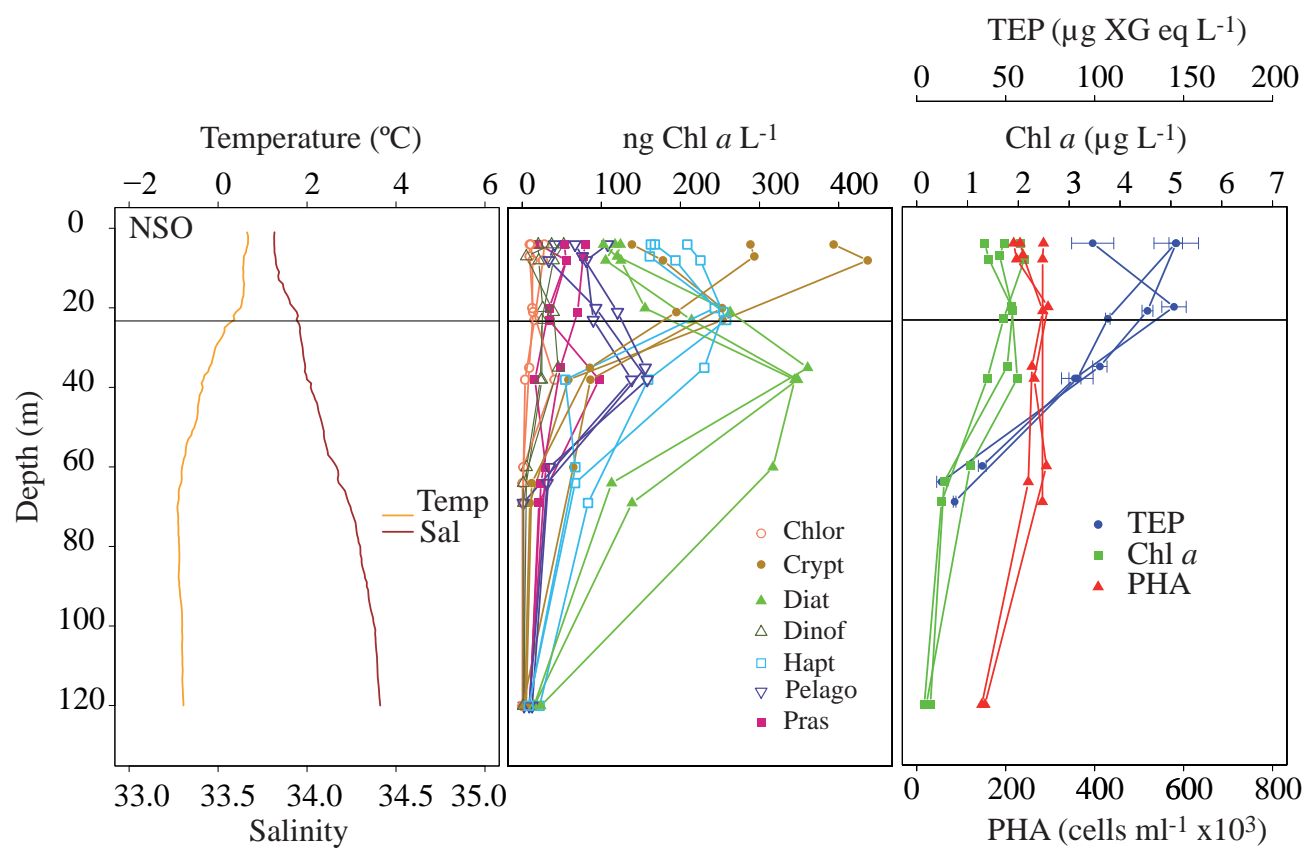
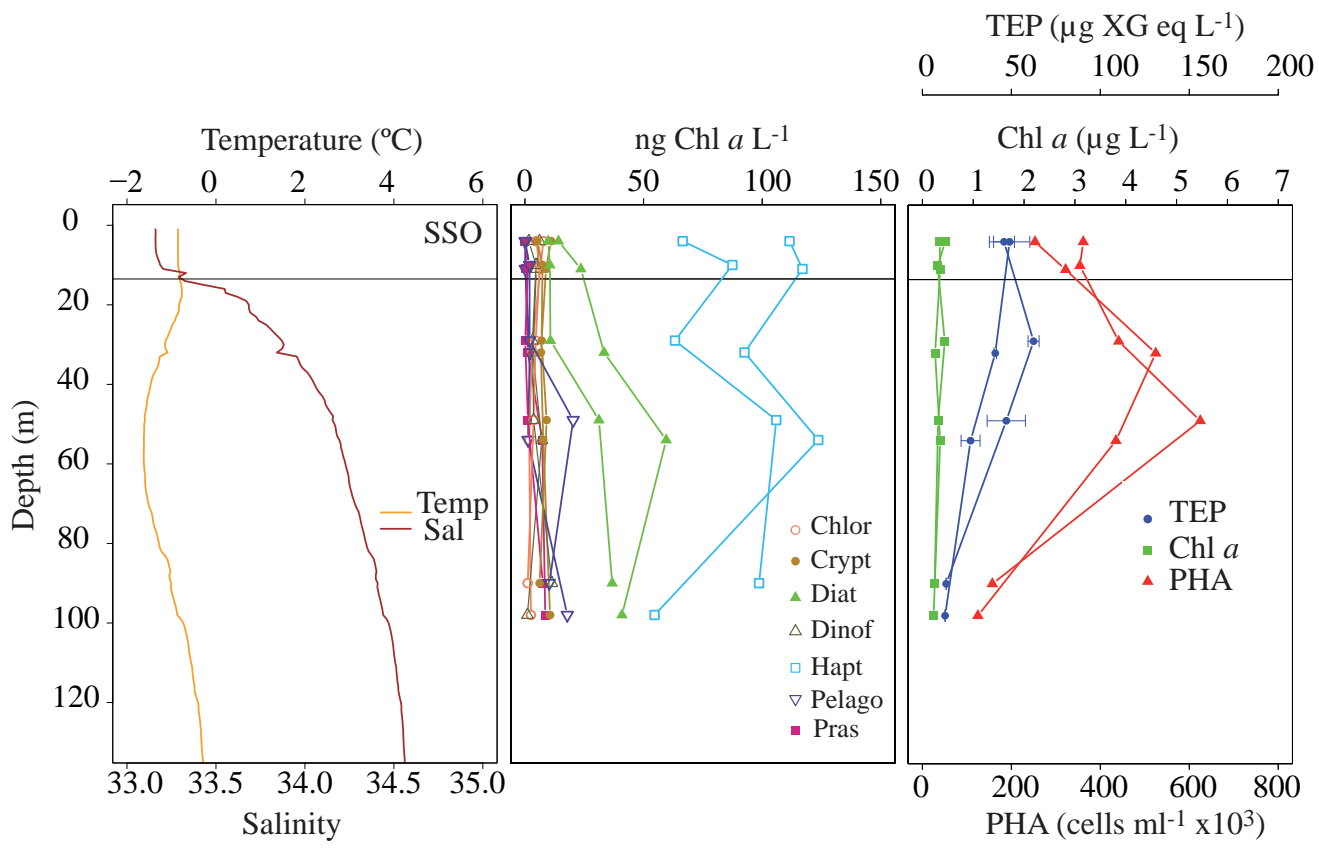
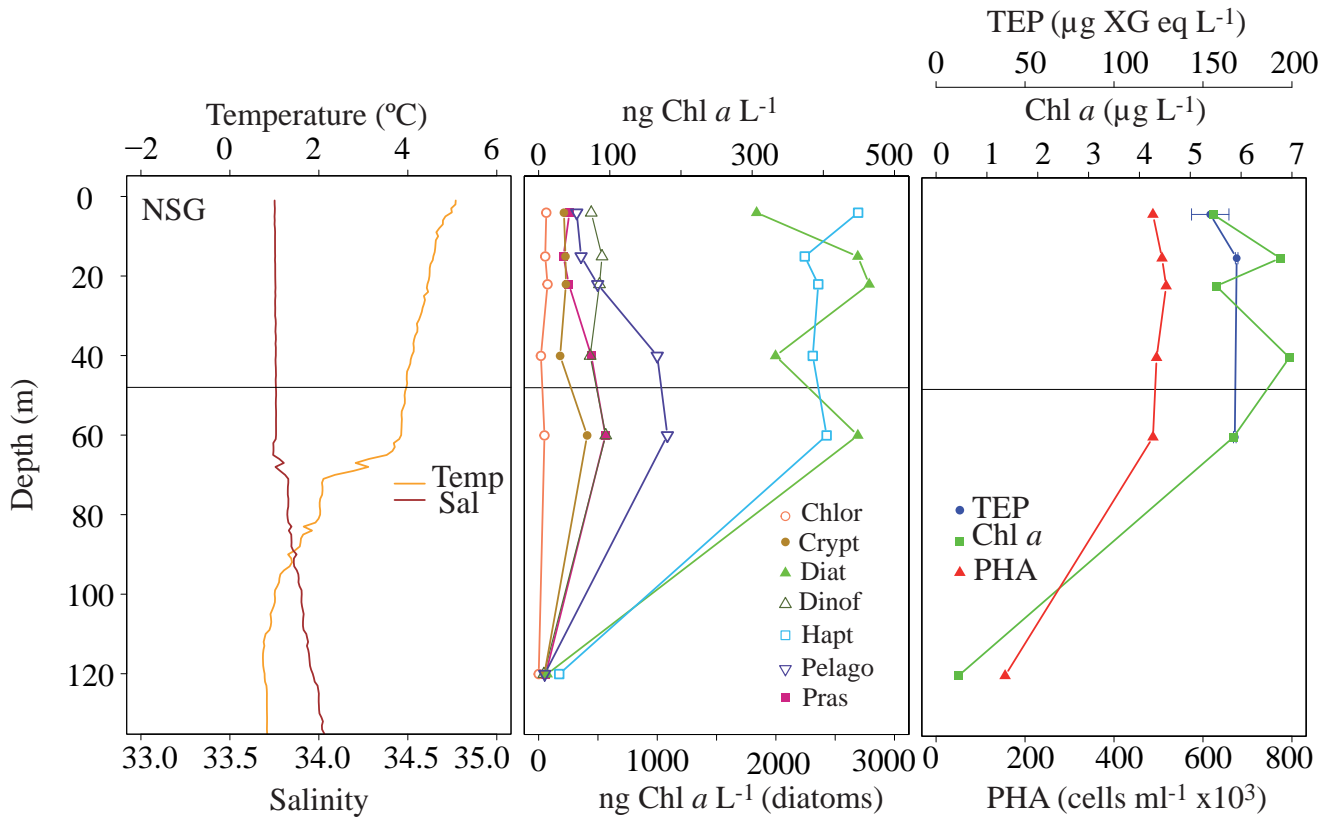


Figure 3







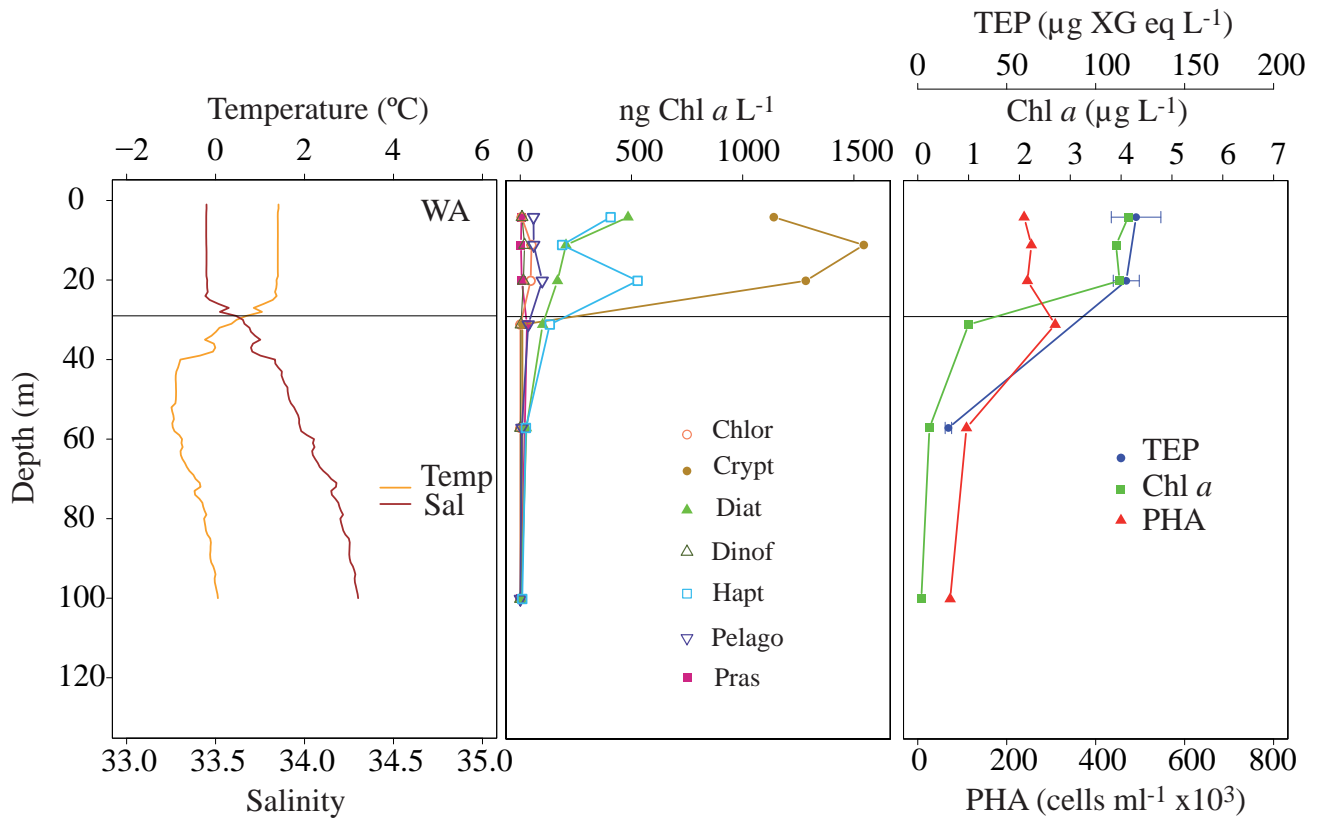


Figure 4

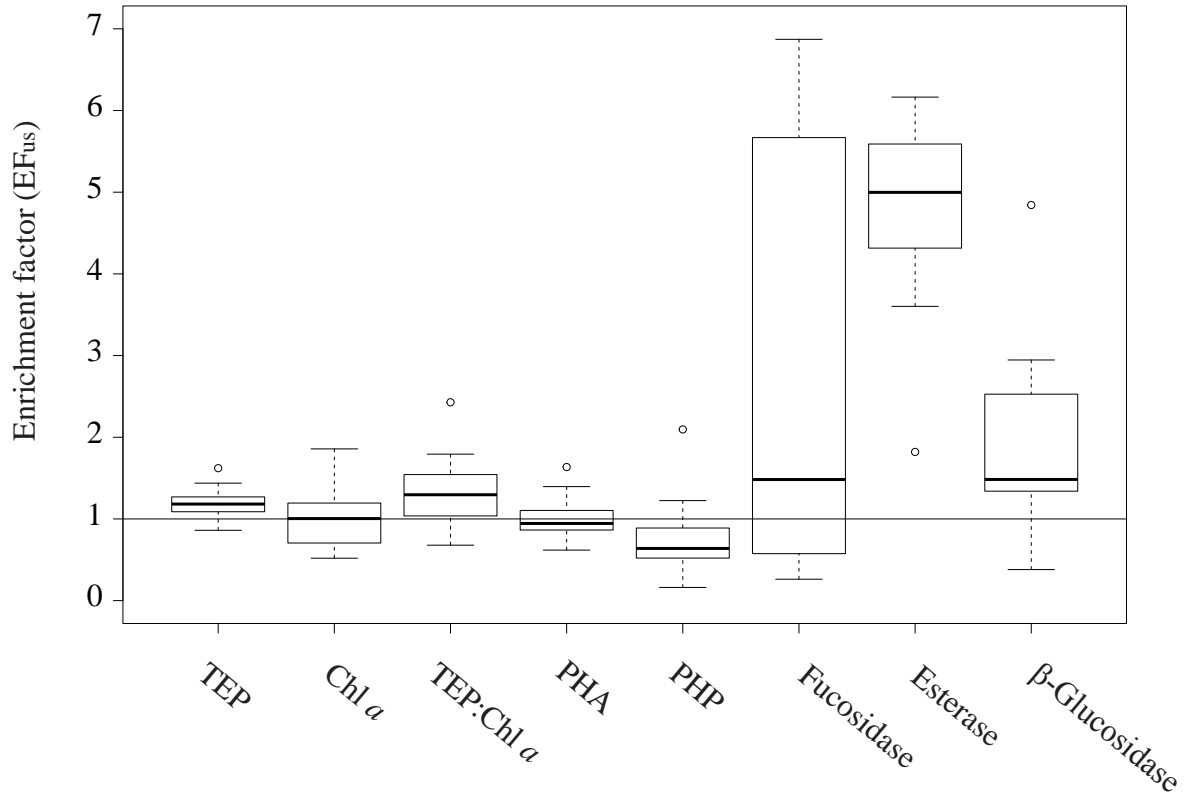


Figure 5

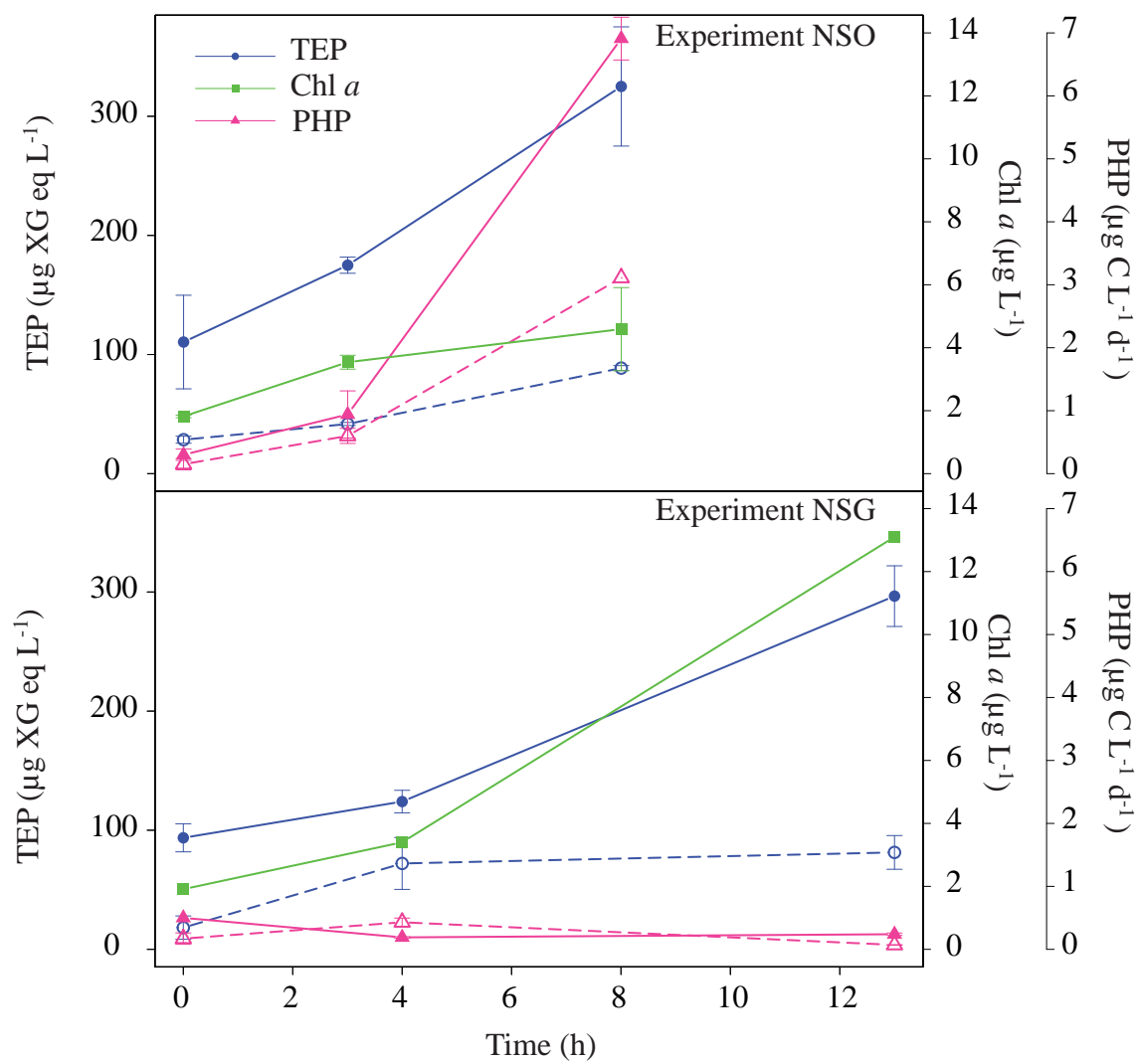


Figure 6

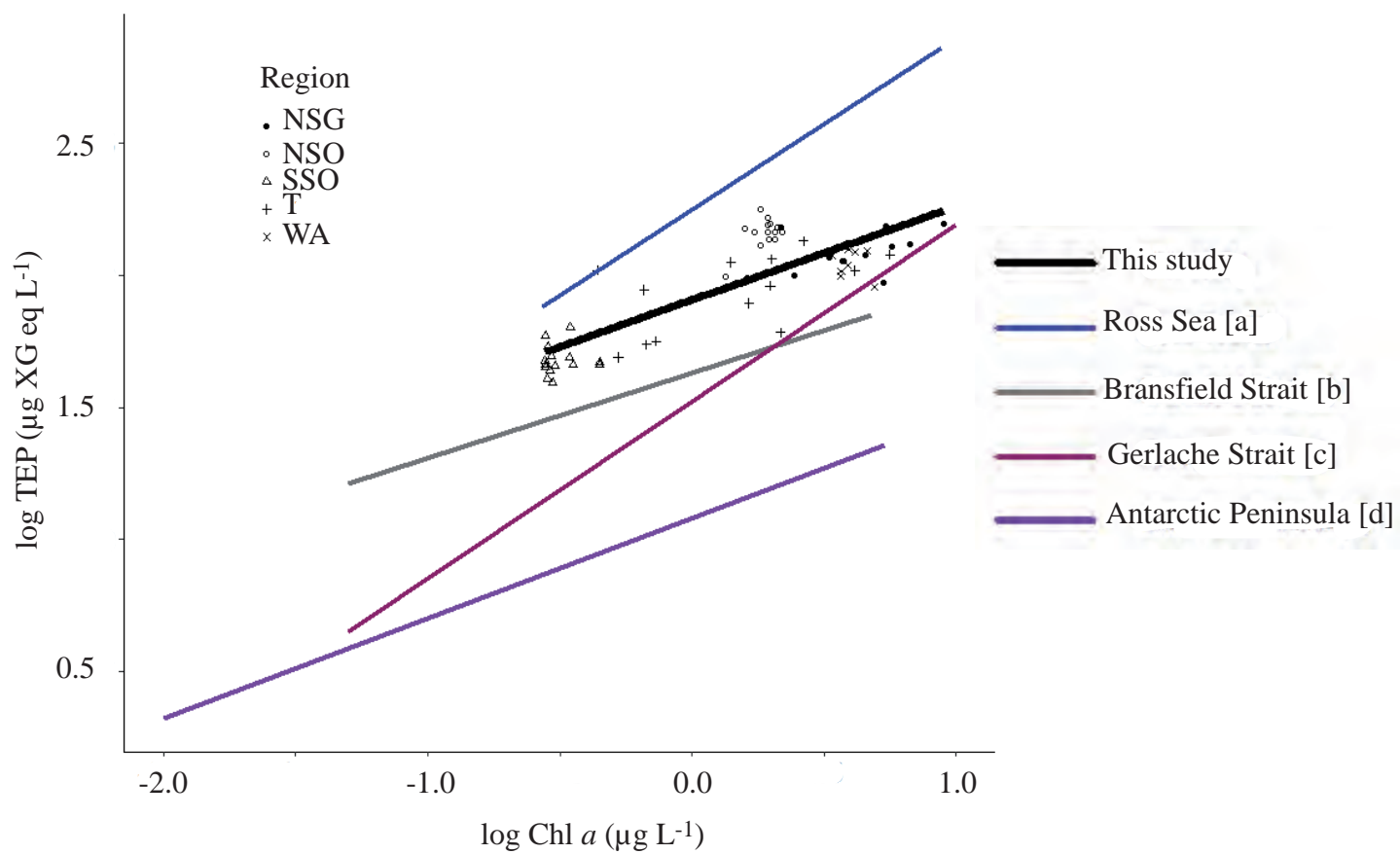


Figure S1

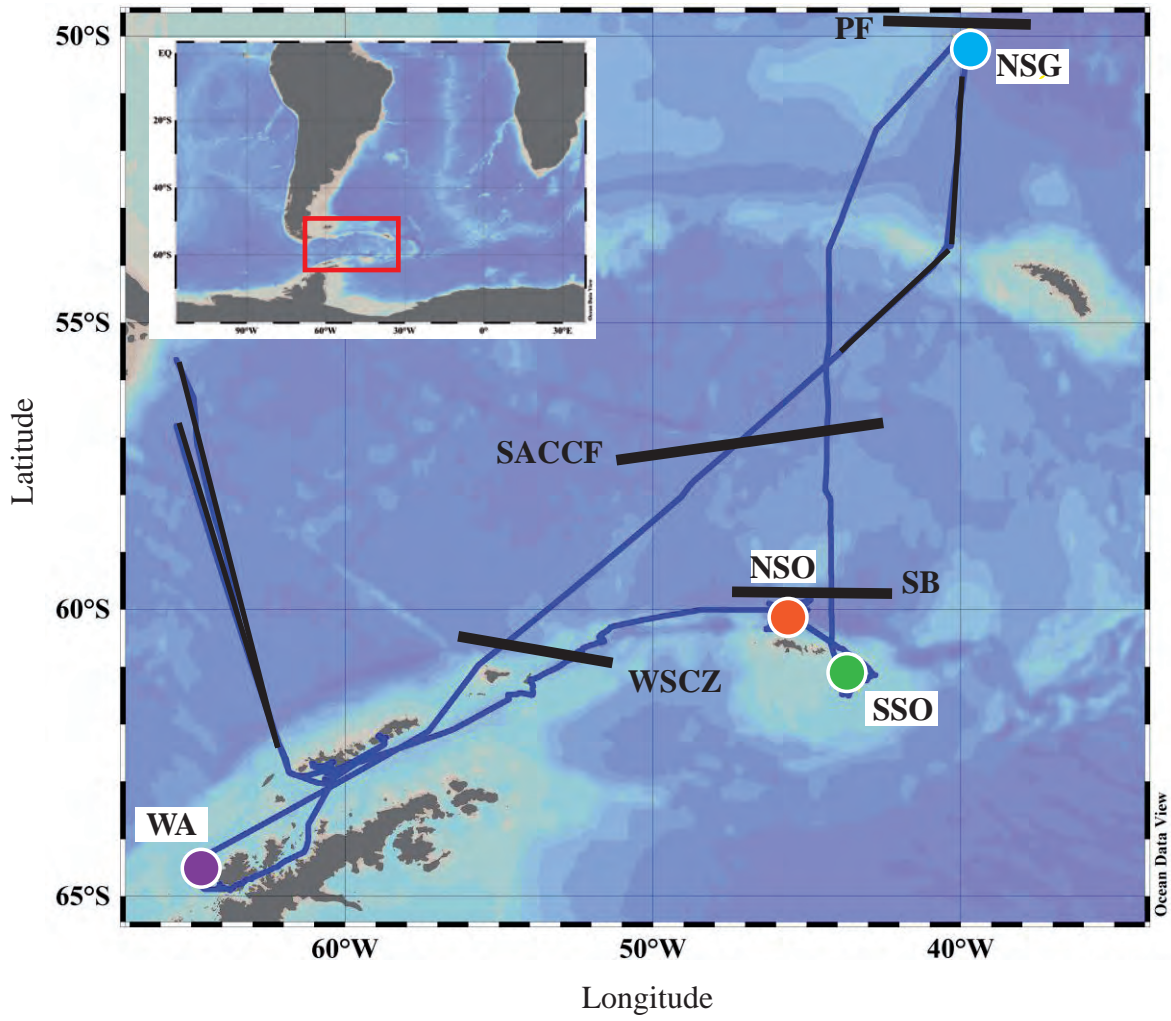


Figure S2

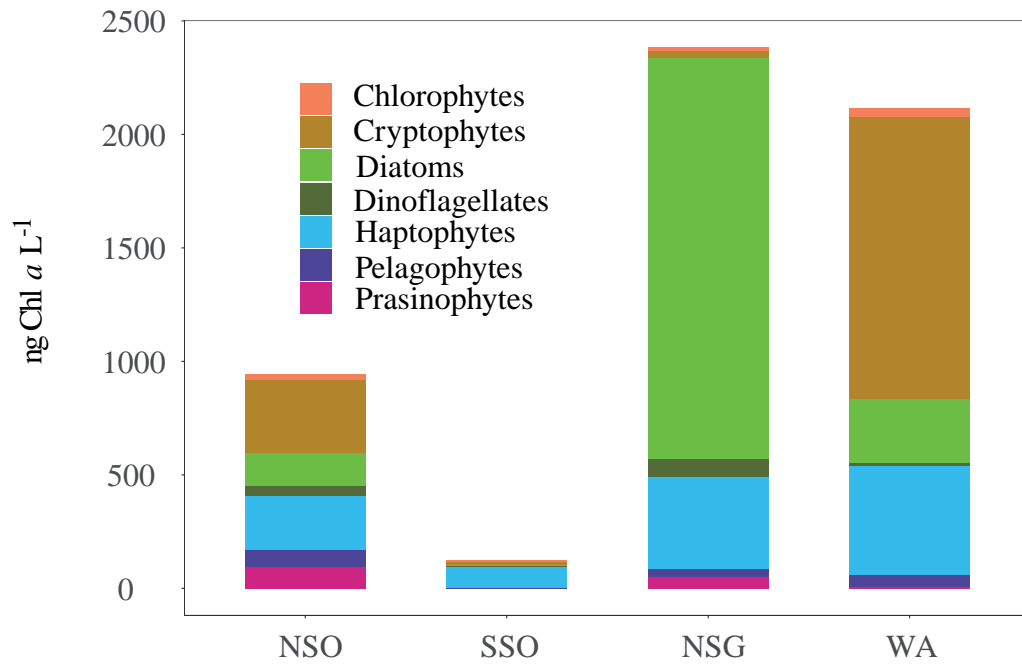


Figure S3

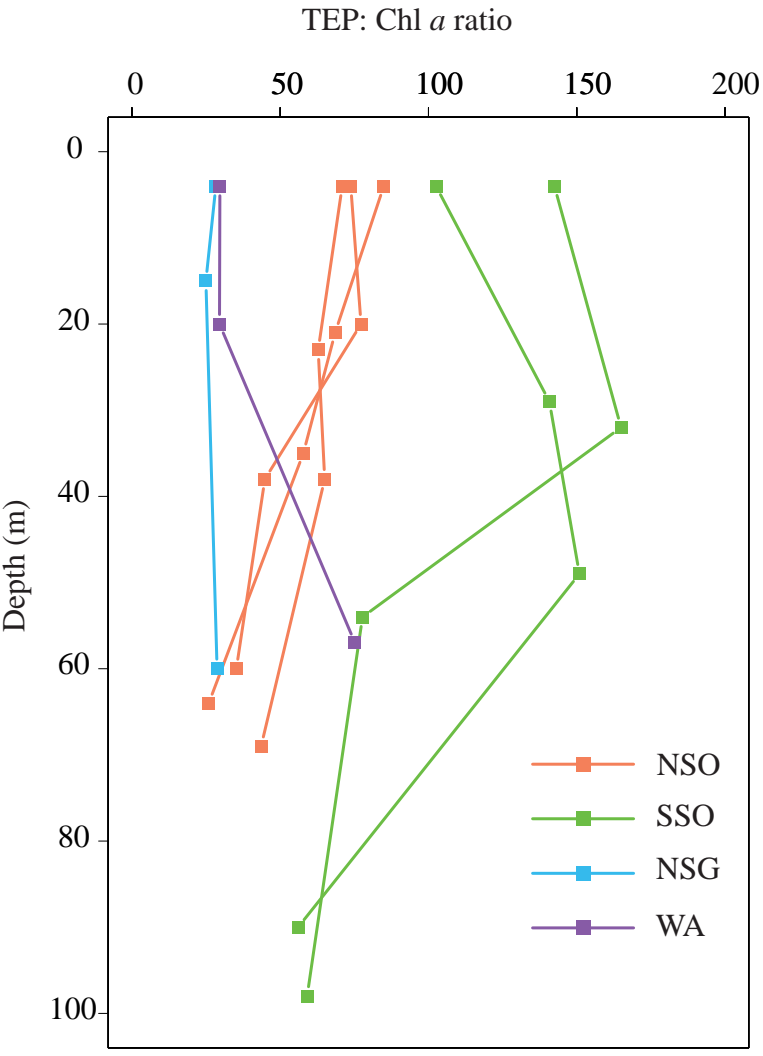


Figure S4

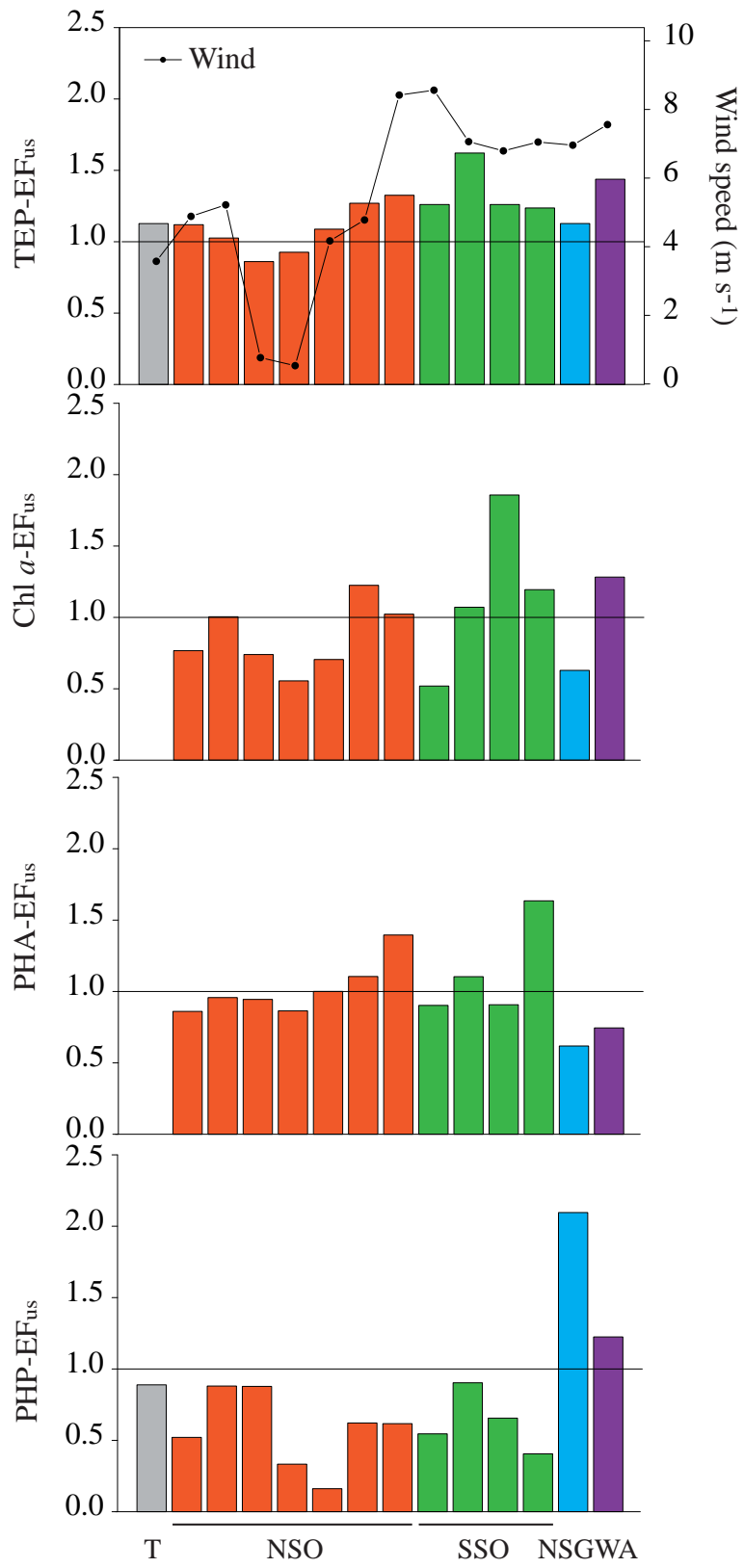


Figure S5

